



Department of Chemistry

1102 Natural Sciences 2  
University of California, Irvine  
Irvine, CA 92697-2025

Dear Editor,

we highly appreciate the constructive comments from the reviewers, and we have addressed the comments in the revised paper. We hope that the following responses are satisfying and that the paper can be accepted for publication in *Atmos. Chem. Phys.* The reviewers' comments have been reproduced in blue text below, followed by our point-by-point replies, and all changes to the manuscript text are also marked in blue in the revised version.

Reviewer comments:

**Reviewer: 1**

This work is based on quantum chemical calculations and kinetic simulation as well as ESI-MS experiments to study the aerosol nucleation abilities for various composition and charge states. The cluster binding patterns with size dependence, the nucleation barrier analysis, the cluster relative concentrations ratio and the formation rates are properly analyzed. The strong binding of guanidine comparing with the other bases is highly emphasized and properly validated. This work provides important insights to the different base contributing nucleation abilities and has shown significant evidences from the view of structure, thermodynamics and kinetics. So I recommend it to be published in *Atmos. Chem. Phys.* with minor revisions.

Specific comments:

1) In 3.3, for the conclusion that "This indicates that the enhancing effect of bisulfate in particle formation becomes more remarkable for weaker bases, since the presence of bisulfate removes the thermodynamic barrier of cluster growth (which does not exist in the case of guanidine)", it is unreasonable to draw this since the analysis for figure 6 only points to the stronger nucleation abilities with the increase of alkalinity for the case of bisulfate. If "the enhancing effect of bisulfate" could be known, it should be compared with different acids with the same base, like comparing figure 6 with figure 2. Whether or not the enhancing effect of bisulfate is more remarkable for weaker bases could also be figured out through comparing figure 6 with figure 2.

**Author reply:**

We agree that this sentence might be confusing. We have moved the sentence to the end of 3.3 and modified it to the following format:

"The enhancing effect of ions in particle formation becomes more remarkable for weaker bases, since the presence of ions allows the cluster growth to occur without thermodynamic barrier (which does not exist in the case of guanidine). The enhancing effect of ions on particle formation rates is presented in Figure 10."

2) For the simulation of formation rates with the aid of ACDC, the boundary condition setting is crucial so the boundary conditions for all the systems should be added on the supplementary information.

**Author reply:**

We thank for the suggestion. We have added the boundary conditions to the supporting information.

3) The overestimation of new particle formation rates with constant base source is a very important conclusion. More descriptions about the constant base concentration case as well as the validity of simulation settings should be given.

**Author reply:**

Modeling of particle formation rates is generally based on the assumptions that the rate is in a steady state, and that the small clusters do not reduce or deplete the vapors. However, these assumptions may not always be valid for real atmospheric situations, which is demonstrated in Figure 11 in terms of the base concentration. Since chamber experiments, such as CLOUD, address steady-state situations, these effects do not concern formation rates measured and modeled for such set-ups. Instead, the two main implications apply to 1) interpretation of field observations, and 2) atmospheric model predictions of vapor concentrations and particle numbers originating from gas-to-particle conversion. First, if observed atmospheric formation events are driven by very strongly clustering species, comparisons with model predictions need to involve explicitly time-dependent cluster formation simulations. Ideally, these include estimates of the vapor sources, if available (see e.g. Hemmilä et al. (2018)). Second, clustering dynamics simulations can also be embedded in an atmospheric model framework for predictions of time-dependent vapor and nanoparticle concentrations given that the computational demand is not too high. These results can also be used to derive approximations for computationally heavier applications, such as large-scale chemical transport and climate models. This is now discussed in Section 3.6.

“While the effects depicted in Figure 11 do not affect steady-state particle formation investigations, such as the CLOUD set-up, they should be considered in the interpretation of field measurements and predictions of ambient aerosol formation, if there is reason to believe that strongly clustering species may be present and their sources can be assessed. Time-dependent clustering simulations can be embedded in, for instance, an atmospheric box model to probe the vapor–cluster exchange dynamics. Such modeling approach can be applied to interpret field observations, and to estimate the vapor sink caused by clustering at different conditions.”

**Technological errors:**

1) I am wondering if the free energies shown on figure 6 are standard Gibbs free energies or the actual concentration-dependent ones. If it's the former case, please correct it to match the figure caption.

**Author reply:**

Figure 6 presents the concentration-dependent Gibbs free energies at a sulfuric acid concentration of  $10^7 \text{ cm}^{-3}$  and the relative base concentrations. The corresponding Gibbs free binding energies, from which the actual Gibbs free energies are calculated, are presented in the supporting information Table S1.

**Reviewer: 2**

This paper reports structures and formation rates for new particles containing sulfuric acid and ammonia, dimethylamine, and guanidine, for neutral and charged clusters. The authors present a number of interesting findings, particularly that clusters can be a non-negligible sink of low-concentration but efficient stabilizing gases. The classification of growth mechanisms as a function of charge state and base is also a valuable contribution, and including these in one paper in one set of conditions helps to clarify the differences between these processes. I enthusiastically recommend publication and hope the authors will consider the following comments:

1) The paper mentions  $pK_b$  but this is not the only measure of base strength. The gas-phase proton affinities of the bases is certainly of relevance here, and makes it easier to separate effects from hydrogen bonding (solution-phase basicity) from effects purely due to site-specific basicity. In these clusters, the enhancing effects are likely a different combination of these two depending on the base, as guanidinium in particular can make significantly more hydrogen bonds than dimethylammonium. Can these results be broken down in this way?

**Author reply:**

This question covers a very important shortcoming in atmospheric clustering studies. We hope to fully respond to this question in a separate publication in the near future. For now, we have added the gas-phase basicities to the Introduction to give an additional measure for base strength.

2) What is the expected role of barriers between each growth step. Particularly for the heavily hydrogen-bonded cage structures formed in the guanidinium clusters, one might expect a substantial barrier (transition state) to addition of an additional monomer as a result of the need to break several strong hydrogen bonds to accommodate the new molecule. The paper mentions barriers several times, but this seems to be in reference to stable minima for given compositions that are uphill from a growth perspective. The presence of large barriers could certainly change the outcome for ammonia, and perhaps for the other two bases as well.

**Author reply:**

Indeed, this paper does not address the possible kinetic barriers between global minimum cluster structures. We agree that such kinetic barriers may be non-negligible, both in cluster formation and decomposition. Thus, especially in the case of strongly-bound cage-like clusters, the subsequent growth as well as the evaporation are slower than our calculations assume. Since investigating all the possible barriers for formation and decomposition reactions is computationally very demanding, the possible activation energy barriers are neglected here as well as in most atmospheric clustering studies. Based on comparisons between experimental and theoretical results, however, the lack of activation barriers in simulations either does not affect remarkably the particle formation rates or is compensated by some other approximation leading to a beneficial cancellation of errors. Specifically, for steady-state particle formation, the role of kinetic barriers is reduced assuming that the cluster formation and decomposition rate coefficients are connected by detailed balance (Eq. (S2)), unless the barriers are strongly composition-dependent. Therefore, in this study we do not speculate on the role of activation energy barriers, but some useful guide can be found e.g. in the studies by DePalma et al. (2014), Xu et al. (2017) and Bzdek et al. (2017). We have added the following in the end of Section 3.5:

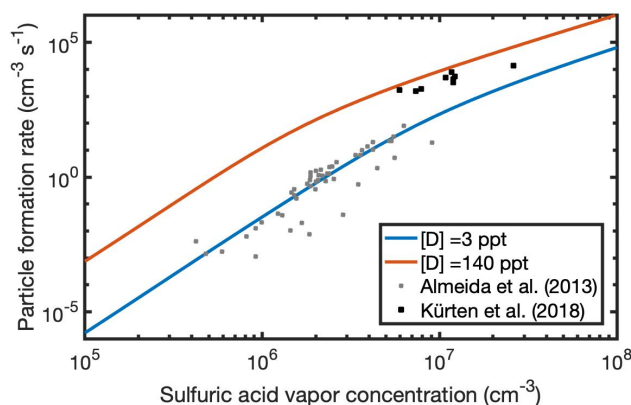
“It should be noted that throughout the paper we have focused on *thermodynamic barriers*. In addition, the cluster growth might be hindered due to *kinetic barriers*. The addition of a monomer or a cluster to a pre-existing cluster might require cluster reorientation which in turn may lead to the breaking of intermolecular bonds, and thus, non-negligible kinetic barriers (DePalma et al., 2014; Bzdek et al., 2017; Xu et al., 2017). Thus, especially in the case of strongly-bound cage-like clusters, the subsequent growth as well as the evaporation may be slower than our calculations assume. For steady-state particle formation, however, the role of kinetic barriers is reduced assuming that the cluster formation and decomposition rate coefficients are connected by detailed balance. Because of this and for the fact that investigating all the possible barriers for formation and decomposition reactions is computationally very demanding, the kinetic barriers are neglected in this study.”

3) Over the range of concentrations studied at CLOUD, the simulations appear to overpredict the formation rates. Can the authors comment on this, particularly since the potential enhancing effects of water and mixed bases are not treated here?

**Author reply:**

The reason for this may actually be an underprediction of the experimental CLOUD particle formation rates by the analysis of Almeida et al. (2013). Kürten et al. (2018) reanalyzed the sulfuric acid-dimethylamine particle formation rates for the data measured earlier at CLOUD using a more advanced method. The reanalysis yielded an order of magnitude higher particle formation rates than previously assessed, and we have now

added these new CLOUD data to Figure 9. The reevaluated particle formation rates show a good agreement with our upper limit simulations ([dimethylamine]=140 ppt<sub>v</sub>). We have updated the figure and added the following:



“In the case of dimethylamine, the measured data points from the study of Almeida et al. (2013) are close to the simulated [D]=3 ppt<sub>v</sub> particle formation rate. However, recently Kürten et al. (2018) reanalyzed that data using a more advanced method. The reanalysis yielded an order of magnitude higher particle formation rates than previously assessed, and the reevaluated particle formation rates show a good agreement with our upper limit simulations [D]=140 ppt<sub>v</sub>.

#### 4) The authors speculate on the role of water, but what about the role of base exchange?

##### Author reply:

We agree that the role of base exchange as well as base synergy is worth of mention and we have added the following paragraph in the Conclusions section:

“Under atmospheric conditions, both ammonia and dimethylamine can be available, and new-particle formation may occur via three-component pathways. This three-component pathway can lead to higher new-particle formation rates than the two-component pathways for two main reasons: 1) base exchange and 2) synergistic effects. 1) For pre-existing sulfuric acid-ammonia clusters, the substitution of ammonia by dimethylamine can be assumed to be fast based on studies by e.g. Bzdek et al. (2017) and Kupiainen et al. (2012). 2) When sulfuric acid-dimethylamine clusters uptake ammonia molecules, the number of intermolecular bonds increases which can further stabilize the clusters and thus make the subsequent cluster growth faster, as we have showed recently (Myllys et al., 2019). The role of base exchange and synergy are yet unresolved in the case of guanidine; however, since guanidine is a stronger base and capable of forming more intermolecular bonds than ammonia or dimethylamine, the reasonable assumption would be that guanidine can replace either ammonia or dimethylamine fast and that the replacement increases the cluster stability and particle formation rate. As sulfuric acid and guanidine form very stable clusters containing a large number of intermolecular bonds, we do not expect that the presence of either ammonia or dimethylamine would enhance the particle formation by synergistic effects.”

Minutae: The term "intermolecular interactions" is used frequently in this paper, but it seems to be primarily referring to hydrogen bonds. Is there a specific reason the use of "hydrogen bond" is avoided here?

##### Author reply:

We have used "intermolecular interactions" since it covers both: the hydrogen bond between neutral electronegative and -positive atoms as well as the ionic bond where the proton transfer has occurred.

On page 3, a reference (gua, 2013) appears to be misformatted.

##### Author reply:

We thank the reviewer for spotting this mistake, and we have corrected the reference.

- Almeida, J., et al.: Molecular Understanding of Sulphuric Acid–Amine Particle Nucleation in the Atmosphere, *Nature*, 502, 359–363, 2013.
- Bzdek, B., et al.: Mechanisms of Atmospherically Relevant Cluster Growth, *Acc. Chem. Res.*, 50, 1965–1975, 2017.
- DePalma, J., et al.: Activation Barriers in the Growth of Molecular Clusters Derived from Sulfuric Acid and Ammonia, *J. Phys. Chem. A*, 118, 11547–11554, 2014.
- Kupiainen, O., et al.: Amine Substitution into Sulfuric Acid–Ammonia Clusters, *Atmos. Chem. Phys.*, 12, 3591–3599, 2012.
- Kürten, A., et al.: New Particle Formation in the Sulfuric Acid–Dimethylamine–Water System: Reevaluation of CLOUD Chamber Measurements and Comparison to an Aerosol Nucleation and Growth Model, *Atmos. Chem. Phys.*, 18, 845–863, 2018.
- Hemmilä, M., et al.: Amines in boreal forest air at SMEAR II station in Finland, *Atmos. Chem. Phys.*, 18, 6367–6380, 2018.
- Myllys, N., et al.: Molecular-Level Understanding of Synergistic Effects in Sulfuric Acid–Amine–Ammonia Mixed Clusters, *J. Phys. Chem. A*, 123, 2420–2425, 2019.
- Xu, J., et al.: Nanoparticles Grown from Methanesulfonic Acid and Methylamine: Microscopic Structures and Formation Mechanism., *Phys. Chem. Chem. Phys.*, 19, 31949–31957, 2017.

# Role of Base Strength, Cluster Structure and Charge in Sulfuric Acid-Driven Particle Formation

Nanna Myllys<sup>1,2</sup>, Jakub Kubečka<sup>2</sup>, Vitus Besel<sup>2</sup>, Dina Alfaouri<sup>2</sup>, Tinja Olenius<sup>3</sup>, James N Smith<sup>1</sup>, and Monica Passananti<sup>2,4</sup>

<sup>1</sup>Department of Chemistry, University of California, Irvine

<sup>2</sup>Institute for Atmospheric and Earth System Research, University of Helsinki

<sup>3</sup>Department of Environmental Science and Analytical Chemistry & Bolin Centre for Climate Research, Stockholm University

<sup>4</sup>Dipartimento di Chimica, Università di Torino

**Correspondence:** Nanna Myllys (nanna.myllys@uci.edu)

**Abstract.** In atmospheric sulfuric acid-driven particle formation, bases are able to stabilize the initial molecular clusters, and thus enhance particle formation. The enhancing potential of a stabilizing base is affected by different factors, such as the basicity and abundance. Here we use weak (ammonia), medium strong (dimethylamine) and very strong (guanidine) bases as representative atmospheric base compounds, and systematically investigate their ability to stabilize sulfuric acid clusters. Using quantum chemistry, we study proton transfer as well as intermolecular interactions and symmetry in clusters, of which the former is directly related to the base strength and the latter to the structural effects. Based on the theoretical cluster stabilities and cluster population kinetics modeling, we provide molecular-level mechanisms of cluster growth and show that in electrically neutral particle formation, guanidine can dominate formation events even at relatively low concentrations. However, when ions are involved, charge effects can stabilize small clusters also for weaker bases. In this case the atmospheric abundance of the bases becomes more important, and thus ammonia is likely to play a key role. The theoretical findings are validated by cluster distribution experiments, as well as comparisons to previously reported particle formation rates, showing a good agreement.

## 1 Introduction

Atmospheric aerosol particles influence human health and global climate (Kulmala et al., 2007). Airborne particles act as condensation nuclei for clouds and can also directly absorb or scatter the incoming radiation, forming a significant but highly uncertain effect on Earth's radiation balance. New-particle formation (NPF) from atmospheric vapors is a significant source of ultrafine particles, but all the participating vapors as well as the molecular-level mechanisms are not fully resolved (Zhang et al., 2012; Hallquist et al., 2009). In the present-day atmosphere that contains high levels of sulfur, sulfuric acid is a key precursor vapor and has been shown to be linked to new-particle formation events in various environments. However, sulfuric acid-driven NPF requires additional stabilizing compounds in order to yield particle formation rates similar to those observed in the atmosphere (Kulmala et al., 2013). These compounds include atmospheric bases and ions (Almeida et al., 2013; Lehtipalo et al., 2016).

The most abundant base in the atmosphere is ammonia with a typical gas-phase concentration at the level from sub-ppb<sub>v</sub> to tens of ppb<sub>v</sub>. A major source of ammonia is agricultural emissions, with other important sources including industry, oceans and vegetation (Anderson et al., 2003). Ammonia has been shown to significantly increase particle formation rates in comparison to the binary sulfuric acid–water system, and is thus expected to be an important player in NPF in at least some environments (Kurtén et al., 2007). Ammonia is a weak base with a dissociation constant  $pK_b$  of 4.75 and a gas-phase basicity of  $-195.7$  kcal/mol, and can stabilize sulfuric-acid-containing molecular clusters by proton transfer reactions and hydrogen bond formation. Amines, on the other hand, are stronger bases than ammonia, and show a much larger stabilization effect (Almeida et al., 2013). Approximately 150 amines have been detected in the atmosphere, with alkylamines being the most abundant at the level of ppt<sub>v</sub> (Ho et al., 2008). Amine emissions are dominated by human activities such as industry, animal husbandry and fish processing, with common natural sources being soils and marine environments (Ge et al., 2011). In recent years, dimethylamine has been the most studied amine in atmospheric particle formation research. It is a medium-strong base with a  $pK_b$  value of 3.27 and a gas-phase basicity of  $-214.3$  kcal/mol. Dimethylamine has been found to enhance new-particle formation in various environments, including Hyytiälä boreal forest in Finland and Shanghai megacity in China (Kulmala et al., 2013; Yao et al., 2018). Also laboratory experiments and computational studies have confirmed that dimethylamine is able to enhance sulfuric acid-driven particle formation rates by up to several orders of magnitude compared to ammonia (Almeida et al., 2013; Olenius et al., 2013; Kurtén et al., 2008; Ahlm et al., 2016; Temelso et al., 2018).

In addition of the commonly studied ammonia and amines, several studies have recently investigated possibilities of other bases to participate in new-particle formation. For instance, diamines, amineoxides and guanidine compounds have been suggested to have a role in the stabilization of sulfuric-acid-containing clusters (Xie et al., 2017; Jen et al., 2016; Elm et al., 2016; Myllys, 2017). In fact, these compounds are able to enhance particle formation much more effectively than ammonia or dimethylamine, however, their atmospheric abundances remain unclear. Multifunctional compounds such as diamines and amineoxides can form more intermolecular interactions than monoamines, and thus the heterodimer formation from acid and base molecules as well as the subsequent cluster growth are more efficient (Elm et al., 2017). Extremely strong organobases, such as guanidine compounds, may interact with sulfuric acid so strongly that the evaporation of clusters is negligible. In this case particle formation becomes fully collision-driven, i.e. occurs without thermodynamic barriers. In our recent computational study, we demonstrated that at similar ambient conditions, guanidine can enhance  $\sim 1$ -nm nanoparticle formation rates by up to several orders of magnitude compared to dimethylamine. We also showed that guanidine requires a significantly lower gas-phase base concentration ( $\sim 2000$  times lower) to reach the same enhancing effect on molecular cluster formation as dimethylamine (Myllys et al., 2018). This implies that even at a very low atmospheric concentration, strong bases might have an important role in the initial steps of particle formation.

There exists a plethora of strong base species, and here we use guanidine, with a  $pK_b$  value of 0.4 (Angyal and Warburton, 1951) and a gas-phase basicity of  $-226.9$  kcal/mol, as a representative strong base. Guanidine may be released to the environment through various waste streams, including the production and use in industry in the manufacture of, e.g., medicines, military munitions, polymeric resins and flame retardants (Kumar et al., 2002; Oxley et al., 2008; Zhao et al., 2015; Kaplan et al., 1982). In addition, guanidine can be released from natural sources as it is a normal product of protein metabolism

(Marescau et al., 1992; Bonas et al., 1963; Van Pilsum et al., 1956; Swick, 1958). As guanidine is a strong base, its volatilization from wet environments can be assumed to be negligible due to guanidinium cation formation. However, the saturation vapor pressure of neutral guanidine is 293 Pa (at room temperature) which indicates that it is likely to volatilize from dry surfaces (The Merck Index, 2013).

5 Ions, a focus of the current study, can enhance cluster binding through strong intermolecular bond formation with electrically neutral molecules. The bisulfate anion or the protonated base in charged sulfuric acid–base clusters can act as a strong conjugate base or acid and suppress the evaporation of especially the smallest clusters. Ions can thus play an important role in the initial steps of NPF, but their relative enhancement with respect to cluster formation from solely electrically neutral molecules depends on the stability of the neutral clusters (Lehtipalo et al., 2016). In addition, charged species can be directly detected by mass  
10 spectrometer techniques, which enables direct comparison of measurements and molecular modeling.

In this paper we apply computational chemistry to comprehensively and systematically investigate the effect of base properties on two-component sulfuric acid–base nanoparticle formation. We consider the strength and abundance of the base, and use ammonia, dimethylamine and guanidine as proxies for weak, medium strong and very strong bases, respectively. We study the role of ion-mediated particle formation in the different sulfuric acid–base systems by including negatively and positively  
15 charged clusters containing a bisulfate anion or a base cation. Electrospray Ionization Atmospheric Pressure interface Time-Of-Flight (ESI-APi-TOF) measurements are performed to further confirm the theoretical findings.

## 2 Computational and Experimental Details

### 2.1 Gibbs Free Energy of Cluster Formation

Determining atmospheric cluster stabilities and their effects on cluster formation kinetics requires calculating the Gibbs free  
20 formation energies. It is generally assumed that the global minimum free energy structures of different cluster compositions dominate atmospheric cluster distributions, and can thus be used to describe the properties of a cluster population. For clusters consisting of several molecules, the potential energy surface becomes highly complicated and finding the global minimum free energy structure is challenging. Here we study acid–base clusters containing 0–4 acid and 0–4 base molecules, including both electrically neutral clusters as well as the corresponding anionic and cationic clusters. We used cluster structures of our  
25 previous studies (Myllys et al., 2018, 2019; Olenius et al., 2013) as a basis for global minimum Gibbs free energy clusters. The structures of clusters not studied before were obtained by a new configurational sampling procedure, as explained in the supporting information. For previously reported cluster structures that seemed to differ from general trends, we conducted a new configurational sampling to test if the global minimum had been found correctly. For anionic clusters, we include compositions in which the number of acid molecules is equal or larger than the number of base molecules, and for cationic  
30 clusters compositions that have an equal or larger number of base molecules compared to acid molecules. This selection saves computational time without affecting the particle formation modeling results, as other types of compositions can be expected to be less stable and thus redundant.

Cluster geometries are optimized and the vibrational frequencies are calculated using  $\omega$ B97X-D/6-31++G\*\* level of theory (Chai and Head-Gordon, 2008; Krishnan et al., 1980). In previous studies,  $\omega$ B97X-D/6-31++G\*\* has been shown to yield good geometries and thermochemical parameters for non-covalently bound molecular clusters (Myllys et al., 2016b). In order to obtain highly accurate binding energies, we calculate electronic energy corrections on top of the DFT structures using a linear-scaling coupled cluster method DLPNO–CCSD(T) with an aug-cc-pVTZ basis set (Riplinger and Neese, 2013; Riplinger et al., 2013, 2016; Kendall et al., 1992). We use tight pair natural orbital criteria, tight self consistent field criteria and integration grid 4 in all coupled cluster calculations (keywords TightPNO, TightSCF, GRID4) (Liakos et al., 2015). We have shown earlier that the DLPNO–CCSD(T)/aug-cc-pVTZ level of theory with TightPNO yields binding energies close to the canonical coupled clusters with a significant gain in computational resources (Myllys et al., 2016a, 2018). All geometries are optimized and vibrational frequencies are calculated using Gaussian 16 RevA.03 (Frisch et al., 2016). Electronic energy corrections are performed in Orca version 4.0.1.2. (Neese, 2012). Thermochemistry is calculated using rigid rotor–harmonic oscillator approximation and Gibbs free energies are presented in kcal/mol and at 298.15 K. For simplicity, we refer to sulfuric acid as A, ammonia as N, dimethylamine as D and guanidine as G, and cluster compositions as e.g. 2D3A, which refers to a cluster of two dimethylamine and three sulfuric acid molecules.

## 2.2 Atmospheric Cluster Dynamics Code

To study cluster formation kinetics and the dynamics of cluster populations, the calculated Gibbs free energies are used as input in Atmospheric Cluster Dynamics Code (ACDC) (McGrath et al., 2012). The detailed theory of ACDC is explained in the supporting information. Briefly, the model simulates nanoparticle formation by solving the cluster distribution considering collision, evaporation and removal processes. The model calculates the rate constants for each process among the population of clusters and vapor molecules, and solves the cluster birth–death equations at given conditions.

## 2.3 ESI-APi-TOF MS Measurements

Charged sulfuric acid clusters with ammonia, dimethylamine and guanidine were generated in laboratory experiments using an electrospray ionizer (ESI) and analysed by an Atmospheric Pressure interface Time Of Flight Mass Spectrometer (APi-TOF MS). Three samples were prepared and used to generate charged clusters: 100 mmol/l sulfuric acid with 100 mmol/l dimethylamine, 100 mmol/l sulfuric acid with 100 mmol/l guanidine, and 100 mmol/l ammonium bisulfate, all the solutions were prepared in 50% methanol and 50% of Milli-Q water. The solutions were sprayed in both negative and positive modes, producing negatively and positively charged clusters, respectively. The charged clusters were detected by the APi-TOF (Tofwerk AG) mass spectrometer operating in both polarities accordingly. The data were analysed using the Matlab-based program TofTools developed at the University of Helsinki. Further details about the APi-TOF and TofTools can be found from study of Junninen et al. (2010).

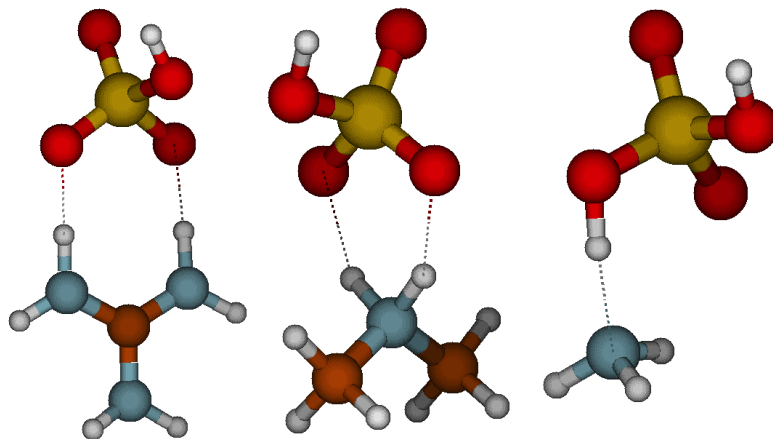


**Figure 1.** Molecular structures of sulfuric acid heterodimers with guanidine (left), dimethylamine (middle) and ammonia (right). Color coding: brown is carbon, blue is nitrogen, red is oxygen, yellow is sulfur and white is hydrogen.

### 3 Results and Discussion

#### 3.1 Acid–Base Heterodimer Formation

The formation of an acid–base heterodimer has been shown to be a crucial step in initial particle formation for many molecular systems (Elm, 2017). Figure 1 shows the molecular structures of the studied heterodimers. In the case of the guanidine and dimethylamine complexes, the proton has transferred from sulfuric acid to base and there are two intermolecular interactions between the acid and the base. Whereas in the guanidine–sulfuric acid complex the hydrogen bonds are linear, i.e. the donor-hydrogen-acceptor angles are close to  $180^\circ$ , in the dimethylamine–sulfuric acid complex the bond angles are  $145\text{--}150^\circ$  which decreases the intermolecular interaction strength compared to straight angles. Therefore, the intermolecular bonds between guanidine and sulfuric acid are much stronger than those between dimethylamine and sulfuric acid. Since ammonia is a weak base, there is no proton transfer in the heterodimer. The ammonia and sulfuric acid molecules form a complex via one hydrogen bond, leading to the binding of sulfuric acid to ammonia being weaker than to dimethylamine or guanidine.

The molecular interaction between the acid and base molecules defines the stability of a formed heterodimer and accordingly its theoretical maximum concentration at given conditions assuming an equilibrium situation. Assuming mass-balance relation for the heterodimer formation reaction leads to the following concentration under equilibrium conditions:

$$15 \quad [(\text{acid})(\text{base})] = [\text{acid}][\text{base}] \frac{k_{\text{B}}T}{P_{\text{ref}}} \exp\left(-\frac{\Delta G_{\text{ref}}}{k_{\text{B}}T}\right) \quad (1)$$

The equilibrium concentration  $[(\text{acid})(\text{base})]$  of the heterodimer is dependent both on the Gibbs free formation energy  $\Delta G_{\text{ref}}$  (calculated at reference pressure  $P_{\text{ref}}$ ) at given temperature  $T$  and on the monomer concentrations  $[\text{acid}]$  and  $[\text{base}]$ . Now we can study how large the magnitude of the exponential Gibbs free energy contribution has relative to the linear concentration factors. The Gibbs free formation energies (at 298.15 K) are  $-6.8$  kcal/mol for ammonia–sulfuric acid,  $-13.5$  kcal/mol for

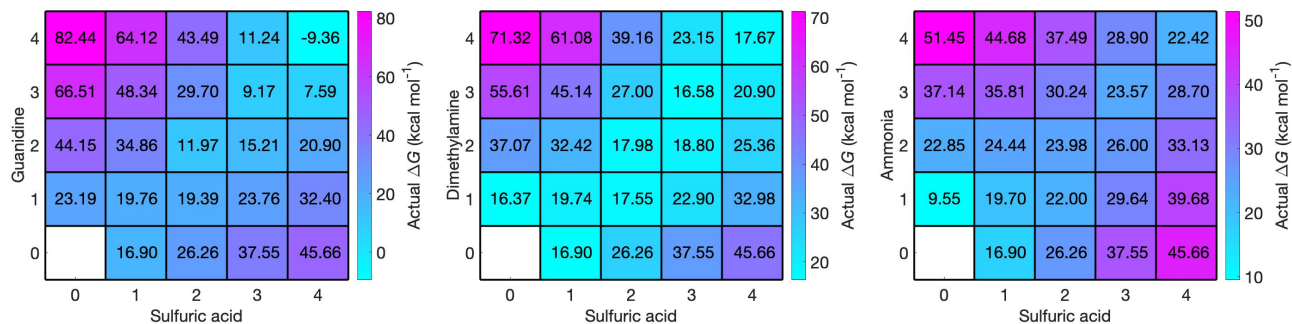


**Figure 2.** Vapor concentration-dependent Gibbs free energies for electrically neutral acid–base clusters at 298.15 K. Sulfuric acid concentration is  $10^7 \text{ cm}^{-3}$  in all cases, and for bases the relative concentrations of [guanidine]= $10^{-5} \text{ ppt}_v$  (left), [dimethylamine]= $1 \text{ ppt}_v$  (middle) and [ammonia]= $10^5 \text{ ppt}_v$  (right) are used.

dimethylamine–sulfuric acid, and  $-20.3 \text{ kcal/mol}$  for guanidine–sulfuric acid dimers. Assuming the same sulfuric acid concentration in all cases, we can calculate what the relative concentrations of ammonia, dimethylamine and guanidine should be to yield the same heterodimer concentration, and obtain  $[G] \approx 1$ ,  $[D] \approx 10^5$  and  $[N] \approx 10^{10}$ . This means that if the atmospheric ammonia concentration is  $10^5 \text{ ppt}_v$ ,  $1 \text{ ppt}_v$  of dimethylamine or  $10^{-5} \text{ ppt}_v$  of guanidine is required to yield a same heterodimer equilibrium concentration as in the case of ammonia. We will refer to these concentrations as relative base concentrations throughout the text.

We have calculated the actual vapor concentration-dependent Gibbs free energies, obtained from the reference values  $\Delta G_{\text{ref}}$  and vapor concentrations through the law of mass action (Eq. (1)), for all acid–base cluster compositions at the relative base concentrations and at a sulfuric acid monomer concentration of  $10^7 \text{ cm}^{-3}$ . At these concentrations, the vapor-dependent Gibbs free energy for all acid–base heterodimers is the same, but Figure 2 shows that further cluster growth is most favorable for guanidine even if its concentration is 5 and 10 orders of magnitude lower than that of dimethylamine and ammonia, respectively. These results demonstrate that, in terms of thermodynamics, the enhancement potential of base in sulfuric-acid-driven clustering is largely dominated by the base strength (characterized by  $\Delta G_{\text{ref}}$ ), and the relative concentration plays only a minor role.

The thermodynamically most favorable clustering pathway for all acid–base systems is close to the diagonal axis, i.e. the actual Gibbs free energy exhibits its lowest values when the number of acid and base molecules is equal, or when the difference between the numbers of acid and base molecules is one. The heterodimer evaporation rates are  $10^5 \text{ s}^{-1}$  for 1N1A,  $1 \text{ s}^{-1}$  for 1D1A and  $10^{-5} \text{ s}^{-1}$  for 1G1A (see the supporting information). This implies that the lifetime of 1N1A is very short and even at an ammonia concentration as high as  $100 \text{ ppb}_v$ , it is unlikely that the concentration of 1N1A heterodimers would be high enough for these clusters to contribute to further cluster growth by coagulation processes. Instead, the growth can be expected to occur via monomeric acid and base additions. The 1D1A cluster has five orders of magnitude lower evaporation rate compared to 1N1A, and this heterodimer is relatively stable. However, because the equilibrium concentration is more than

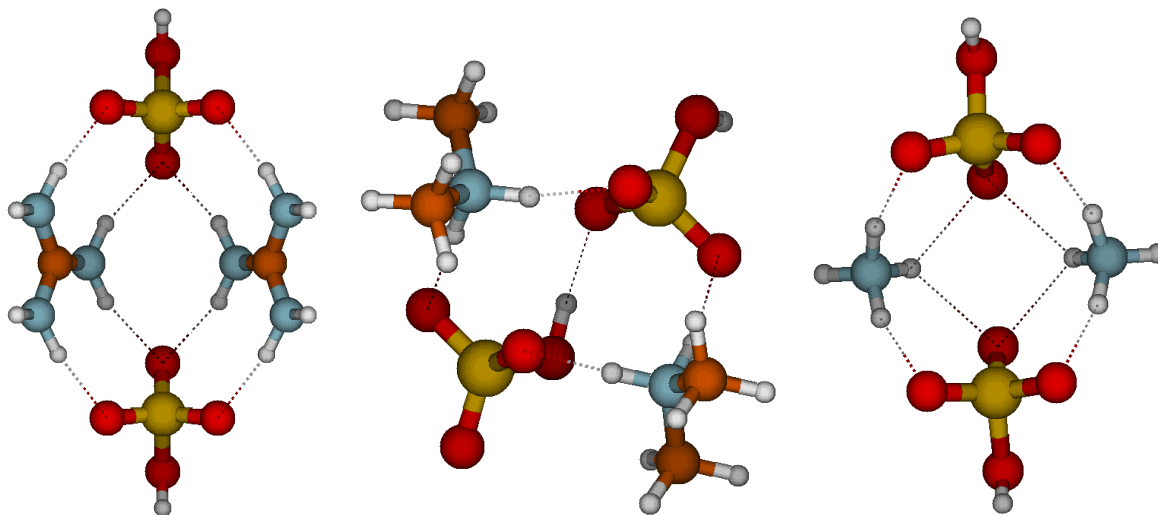


**Figure 3.** Molecular structures of clusters containing two sulfuric acid and two base molecules for guanidine (left), dimethylamine (middle) and ammonia (right). Color coding: brown is carbon, blue is nitrogen, red is oxygen, yellow is sulfur and white is hydrogen.

two orders of magnitude lower than that of monomers, cluster collisions with monomers are still much more likely than those involving 1D1A clusters. The evaporation rate of the 1G1A heterodimer is very low, and therefore heterodimer coagulations are expected to make a major contribution to the growth of sulfuric acid–guanidine clusters. Since each addition of 1G1A to a pre-existing diagonal cluster leads to a lower actual free energy and the cluster evaporation is negligible, the only limiting  
 5 factor to particle formation in this system is the collision frequency between sulfuric acid and guanidine molecules.

### 3.2 Diagonal Cluster Structures

The reason that the clusters along the diagonal are most stable is shown in the cluster structures (Figure 2), in which all sulfuric acid molecules are able to donate a proton to a base molecule. The intermolecular interactions between bisulfate anions and protonated base cations are stronger than those between molecules with no proton transfers. Figure 3 shows the molecular  
 10 structures of 2(acid)2(base) clusters. In all cluster structures, there are two proton transfer reactions from sulfuric acid to base. Ammonia- and guanidine-containing clusters resemble each other in the way that there are eight intermolecular interactions between bisulfate and guanidinium or ammonium ions, the hydroxyl groups of both bisulfates remain free, and the structures have a  $C_{2v}$  symmetry. In the 2G2A structure, the hydrogen bond angles are  $160^\circ$  in the inner circle and  $170^\circ$  in the outer circle, whereas in the 2N2A cluster they are  $120^\circ$  and  $160^\circ$ , respectively. This means that in the 2N2A cluster, the hydrogen bonds in  
 15 the inner circle are very weak. The molecular structure of the 2D2A cluster differs remarkably from that of 2G2A and 2N2A: 2D2A contains five intermolecular interactions and one of them is between the two bisulfates through the free hydroxyl group and the oxygen atom moieties.

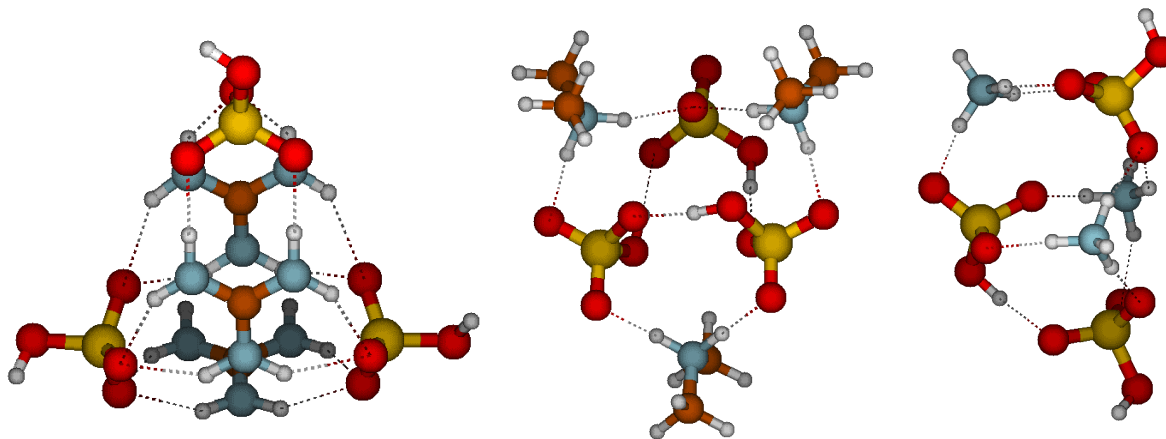


**Figure 4.** Molecular structures of clusters containing three sulfuric acid and three base molecules for guanidine (left), dimethylamine (middle) and ammonia (right). Color coding: brown is carbon, blue is nitrogen, red is oxygen, yellow is sulfur and white is hydrogen.

The Gibbs free binding energies are  $-28.9$  kcal/mol for 2N2A,  $-48.6$  kcal/mol for 2D2A and  $-68.2$  kcal/mol for 2G2A. For 2N2A and 2D2A the dominant evaporation channel is the decomposition to 2(acid)1(base) + free base parties, with evaporation rate constants of  $5 \times 10^4$  and  $3 \times 10^{-3} \text{ s}^{-1}$ , respectively. For the 2G2A cluster, the main decomposition pathway is different: the evaporation of a base molecule would require a proton transfer and breaking of four strong intermolecular interactions, whereas breaking into two 1G1A parts does not require proton transfer reactions but only the breaking of four intermolecular interactions. The dominant evaporation pathway for 2G2A is thus decomposition into heterodimers, with a rate constant of  $3 \times 10^{-11} \text{ s}^{-1}$ .

All 3(acid)3(base) clusters exhibit three proton transfers (Figure 4). In the 3N3A cluster structure, each ammonium ion forms three intermolecular interactions with a bisulfate. In addition there is one intermolecular bond between bisulfate anions. The main decomposition pathway, with a rate constant of  $30 \text{ s}^{-1}$ , is via ammonia evaporation which requires one proton transfer and the breaking of three intermolecular interactions. In the 3D3A structure, each dimethylaminium interacts with two bisulfates via two intermolecular bonds. In addition, all bisulfates interact with two other bisulfates and thus each bisulfate forms four intermolecular bonds. The main evaporation route of 3D3A is via evaporation of dimethylamine at a rate of  $4 \times 10^{-4} \text{ s}^{-1}$ , requiring that a dimethylaminium donates a proton back to bisulfate and two intermolecular interactions are broken. In the case of guanidine-containing clusters, two guanidinium and two bisulfate ions form six intermolecular bonds and one guanidinium and one bisulfate form only four. Assuming that hydroxyl groups can freely rotate at room temperature, the 3G3A cluster is  $C_s$  symmetric. The main evaporation pathway for 3G3A is the decomposition into 1G1A and 2G2A, which requires breaking six intermolecular bonds, and the evaporation rate is  $3 \times 10^{-7} \text{ s}^{-1}$ .

Finally, Figure 5 presents the molecular structures of 4(acid)4(base) clusters, in which four proton transfer reactions occur. In the case of the 4N4A cluster, all ammonium ions form three intermolecular bonds with bisulfate and *vice versa*. In the 4D4A cluster each bisulfate anion interacts with another bisulfate via two intermolecular bonds and the cluster contains a centre

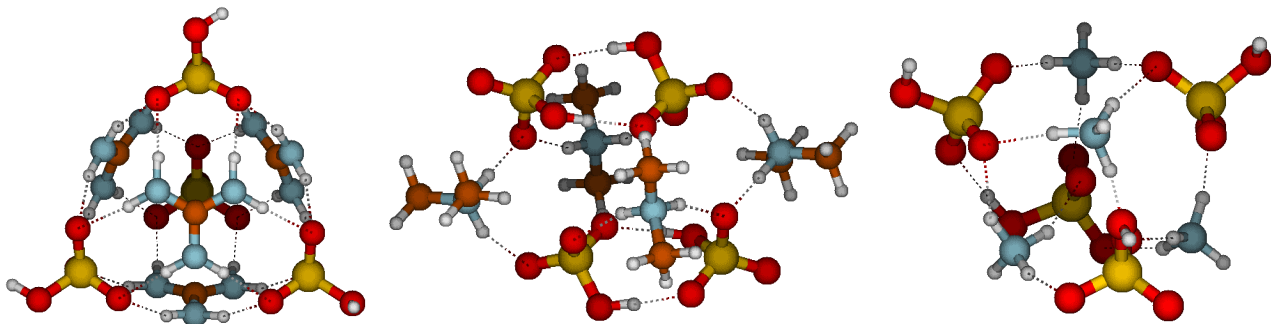


**Figure 5.** Molecular structures of clusters containing four sulfuric acid and four base molecules for guanidine (left), dimethylamine (middle) and ammonia (right). Color coding: brown is carbon, blue is nitrogen, red is oxygen, yellow is sulfur and white is hydrogen.

of inversion, thus belonging to the  $C_i$  point group. All dimethylaminium ions form two intermolecular bonds with bisulfate moieties. In the 4G4A structure, each bisulfate interacts with three guanidinium ions and forms a total of six intermolecular bonds, and *vice versa*. The structure is mesh-like with free hydroxyl groups pointing out of the core. Assuming free rotation of hydroxyl groups at room temperature, the 4G4A cluster belongs to the  $T_d$  point group. The main decomposition pathway of the 4N4A cluster is the evaporation of ammonia with a rate of  $6 \times 10^{-2} \text{ s}^{-1}$ . 4D4A has two equally fast decomposition routes, evaporation into 1D1A + 3D3A or into two 2D2A parts, and its total evaporation rate is  $7 \times 10^{-4} \text{ s}^{-1}$ . The main evaporation pathway for 4G4A is to decompose into two 2G2A parts at a rate of  $2 \times 10^{-15} \text{ s}^{-1}$ . The overall evaporation rates for all clusters are presented in the supporting information in Figure S1.

We have simulated electrically neutral particle formation rates based on the calculated Gibbs free energies using the ACDC model and compared the results to atmospheric measurements (see the supporting information Figure S2). We investigated which simulated base concentrations yield NPF rates close to the atmospheric observations when including only electrically neutral two-component clusters. We found that guanidine concentrations of 0.001–1 ppt<sub>v</sub>, dimethylamine concentrations of 0.1–100 ppt<sub>v</sub> and ammonia concentrations of  $10^4$ – $10^7$  ppt<sub>v</sub> are needed to yield NPF rates of the magnitude of the observations. However, these results do not take ions or hydration into account, which are expected to increase the particle formation rate, especially in the case of ammonia. In addition, synergistic effects between different bases may play a role in the atmosphere. For example, it has been demonstrated that the presence of ammonia increases particle formation when added to a two-component sulfuric acid–amine system (Myllys et al., 2019; Yu et al., 2012; Glasoe et al., 2015).

### 3.3 The Role of Ions in the First Steps of Acid–Base Particle Formation

In addition to proceeding through electrically neutral pathways, atmospheric cluster formation can be ion-induced (Wagner et al., 2017; Kirkby et al., 2016). Sulfuric acid can be deprotonated in the atmosphere by generic air ions to form a bisulfate, here referred to as B. A bisulfate can form a 1A1B complex with a neutral sulfuric acid molecule, the formation free energy of which is highly exergonic ( $-33.8 \text{ kcal/mol}$ ), corresponding to an evaporation rate as low as  $10^{-14} \text{ s}^{-1}$ . Thus a large fraction of

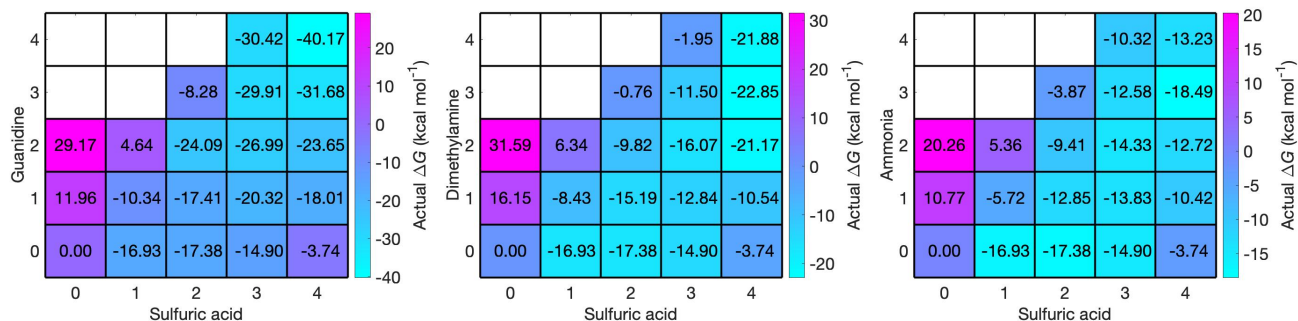


**Figure 6.** Concentration-dependent Gibbs free energies for bisulfate-containing acid–base clusters at 298.15 K. Sulfuric acid concentration is  $10^7 \text{ cm}^{-3}$  in all cases, and for bases the relative concentrations of [guanidine]= $10^{-5}$  ppt<sub>v</sub> (left), [dimethylamine]=1 ppt<sub>v</sub> (middle) and [ammonia]= $10^5$  ppt<sub>v</sub> (right) are used. Note that the  $x$  and  $y$  axes refer to the numbers of neutral acid and base molecules and each cluster contains one bisulfate anion.

bisulfate can be expected to exist as a complex with sulfuric acid, and this complex can grow further by uptake of acid or base molecules. The addition of a second sulfuric acid molecule is the most favorable reaction with a formation free energy of  $-17.4$  kcal/mol. The reaction free energies for addition of guanidine, dimethylamine or ammonia are  $-16.6$  kcal/mol,  $-7.9$  kcal/mol, and  $1.7$  kcal/mol, respectively. This means that the only reaction competitive to the addition of sulfuric acid is the addition of

5 guanidine. The total evaporation rates of the resulting complexes are  $10^{-2} \text{ s}^{-1}$  for 2A1B,  $5 \times 10^{-2} \text{ s}^{-1}$  for 1A1B1G,  $8 \times 10^4 \text{ s}^{-1}$  for 1A1B1D and  $10^{12} \text{ s}^{-1}$  for 1A1B1N. We can again study the vapor-dependent Gibbs free energies using the relative base concentrations, shown in Figure 6. The thermodynamically most favorable formation pathways of negative sulfuric acid–base clusters are below the diagonal axis, corresponding to clusters that contain more acid than base molecules. In the case of guanidine, there is no thermodynamic barrier for cluster growth along the most favorable pathway, and for dimethylamine

10 and ammonia only small barriers can be found around compositions including 1 bisulfate ion, 1 base and 2–3 sulfuric acid molecules. This indicates that the enhancing effect of bisulfate in particle formation becomes more remarkable for weaker bases, since the presence of bisulfate removes the thermodynamic barrier of cluster growth (which does not exist in the case of guanidine):

The base molecules can become ionized in the atmosphere by receiving a proton, here referred to as P, and form guanidinium

15 1G1P, dimethylaminium 1D1P and ammonium 1N1P cations. Protonated bases are likely to form a complex with their own conjugate base, the formation free energies for which are  $-18.3$  kcal/mol for 2G1P,  $-15.7$  kcal/mol for 2D1P and  $-19.1$  kcal/mol for 2N1P. These protonated base dimers are likely to uptake a sulfuric acid molecule with reaction free energies of  $-31.0$  kcal/mol for 1A2G1P,  $-24.9$  kcal/mol for 1A2D1P and  $-16.5$  kcal/mol for 1A2N1P, and the evaporation rates for these clusters are  $10^{-10} \text{ s}^{-1}$ ,  $4 \times 10^{-8} \text{ s}^{-1}$  and  $7 \times 10^{-2} \text{ s}^{-1}$ , respectively. All  $n(\text{acid})n(\text{base})1(\text{protonated base})$  clusters are stable

20 against evaporation for guanidine and dimethylamine. Positive acid–ammonia clusters are somewhat less stable, but still have considerably lower evaporation rates than their neutral equivalents. Figure 7 shows the concentration-dependent Gibbs free

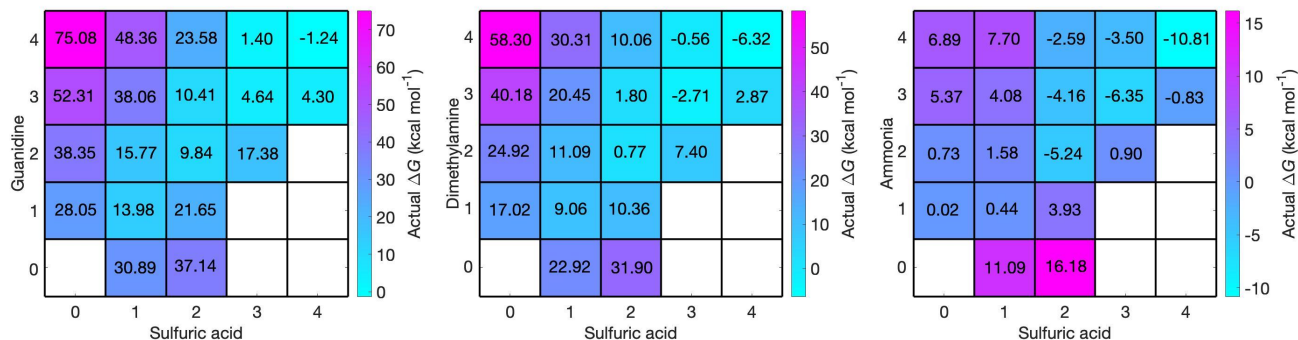


**Figure 7.** Concentration-dependent Gibbs free energies for protonated-base-containing acid–base clusters at 298.15 K. Sulfuric acid concentration is  $10^7 \text{ cm}^{-3}$  in all cases, and for bases the relative concentrations of [guanidine]= $10^{-5}$  ppt<sub>v</sub> (left), [dimethylamine]=1 ppt<sub>v</sub> (middle) and [ammonia]= $10^5$  ppt<sub>v</sub> (right) are used. Note that the  $x$  and  $y$  axes refer to the numbers of neutral acid and base molecules and each cluster contains one protonated base cation.

energies of these positively charged clusters at the relative base concentrations. In all cases, the lowest free energy path is on the diagonal axis, and the cluster formation along it is barrierless, although some barriers are related to growth around the diagonal compositions by monomer additions. The enhancing effect of ions in particle formation becomes more remarkable for weaker bases, since the presence of ions allows the cluster growth to occur without thermodynamic barrier (which does not exist in the case of guanidine). The enhancing effect of ions on particle formation rates is presented in Figure 10.

### 3.4 Charged Cluster Distributions

In experiments performed at the Cosmics Leaving OUtdoor Droplets (CLOUD) chamber as well as in other chamber experiments the clusters involved in NPF are often detected using an Api-TOF or a Chemical Ionization Api-TOF mass spectrometer (Almeida et al., 2013). However, only charged clusters can be directly detected by MS, therefore understanding the stability of both charged and neutral clusters can help to interpret the experimental data. Figure 8 shows the relative ionic acid–base cluster abundance measured using ESI-Api-TOF in the laboratory studies of this work. Since the charged clusters are produced from the liquid phase (Section 2.3), the absolute gas-phase concentrations are challenging to define accurately. Therefore, we use the cluster ratio instead of the absolute concentration to characterize the cluster distribution. The cluster ratio for negatively charged clusters is calculated as  $\frac{[\text{cluster}]}{[\text{bisulfate}]}$ , meaning that the relative concentration of 1B is set to be 1. In the case of positively charged guanidine and dimethylamine clusters, the relative cluster concentrations are calculated based on protonated bases (1G1P and 1D1P) as  $\frac{[\text{cluster}]}{[\text{protonated base}]}$ , and for positively charged ammonia clusters, due to the absence of 1N1P in the mass spectrum, cluster ratio is calculated based on the smallest cluster detected as  $\frac{[\text{cluster}]}{[1A1N1P]}$ .

As discussed above, the interaction between bisulfate and sulfuric acid is very strong, and thus small anionic sulfuric acid clusters are very stable, having the largest relative concentrations in all cases. Guanidine is the only base with an interaction

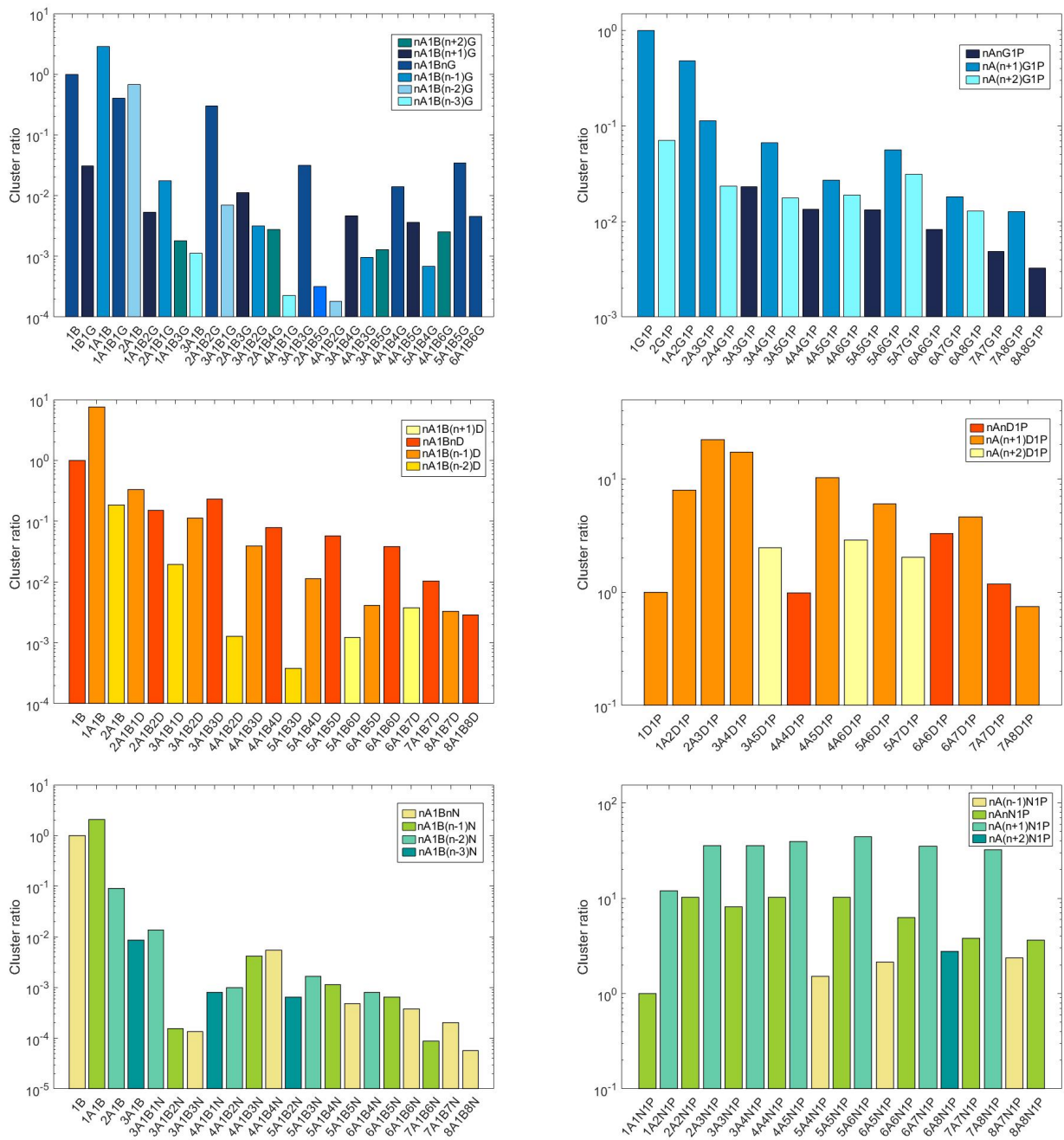


**Figure 8.** Experimentally determined relative cluster concentrations in negative (left) and positive (right) modes for sulfuric acid with guanidine (top), dimethylamine (middle) and ammonia (bottom).

strength with small anionic sulfuric acid clusters comparable to that of sulfuric acid, and thus 1B1G and 1B1AnG clusters can be detected. In the case of ammonia and dimethylamine, the smallest anionic base-containing clusters are 3A1B1N and 2A1B1D, respectively. The most abundant guanidine-containing clusters have the composition  $nA1BnG$ , and are detected up to  $n=6$ . Also clusters with a larger number of base compared to acid ( $nA1B(n+1)G$  and  $nA1B(n+2)G$ ) can be detected. The negatively charged clusters consisting of dimethylamine and sulfuric acid are predicted to be less stable than the guanidine-sulfuric acid clusters (e.g. the evaporation rate for 4A1B4G is  $2 \times 10^{-9} \text{ s}^{-1}$ , and for 4A1B4D, it is eight orders of magnitude higher,  $2 \times 10^{-1} \text{ s}^{-1}$ ). Accordingly, for dimethylamine, a smaller number of clusters is detected. The most abundant clusters are  $nA1BnD$  and  $nA1B(n-1)D$ , similar to the trend observed for the computational results, and clusters up to  $n=8$  are detected. Similarly to guanidine,  $nA1B(n+1)D$  clusters are also observed, but only for  $n \geq 5$ . However, for ammonia, anionic clusters only with equal or smaller number of ammonia than sulfuric acid molecules are stable enough to be detected. These cover sizes from 3A1B1N to 8A1B8N.

In the negative mode, we always observe the formation of the sulfuric acid-bisulfate complex (1A1B). In the positive mode, the formation of 2(base)1P complex is also thermodynamically the most favorable first step in cluster formation and 2(base)1P clusters have low evaporation rates, but we observe the pure dimer cluster only for guanidine (2G1P). The absence of 1N1P and 2N1P in the mass spectrum is likely to be due to instrument limitation: the sensitivity of the instrument has been demonstrated to decrease dramatically for low mass-to-charge ratios (Heinritzi et al., 2016). The absence of 2D1P in the mass spectrum could be explained by the rapid formation of 1A2D1P, which is detected. As the theoretical data show, the addition of sulfuric acid to 2D1P is thermodynamically highly favorable ( $-24.9 \text{ kcal/mol}$ ), and the evaporation rate of 1A2D1P is seven orders of magnitude lower than that of 2D1P. In general, a larger number of clusters is observed in the negative than in the positive mode for all the analysed acid-base clusters. In the positive mode, most of the observed clusters contain more than 4 acids and 4 bases. In all cases, the diagonal clusters  $n(\text{acid})(n+1)(\text{base})1P$  are the most abundant, which is in agreement with theoretical results. Also  $nA nN1P$  clusters are detected in the case of ammonia, whereas for dimethylamine and guanidine, the first detectable clusters below the diagonal axis are 4A4D1P and 3A3G1P, respectively. In addition, cationic clusters with two more neutral acid than base molecules ( $nA(n-1)N1P$ ) are detected only for ammonia. This could be explained by the fact that, in general, sulfuric acid forms more stable positively charged clusters with ammonia compared to dimethylamine and guanidine (e.g., the evaporation rates for 1A1N1P, 1A1D1P and 1A1G1P are  $6 \times 10^{-1}$ ,  $2 \times 10^3$  and  $10^4 \text{ s}^{-1}$ , respectively).

### 3.5 Ion-Mediated Particle Formation

The roles of ammonia and dimethylamine in sulfuric-acid-driven NPF in the presence of ions have been studied in many laboratory experiments. Here we use our full cluster sets including both neutral and charged clusters, and compare the simulated NPF rates against those observed at the CLOUD chamber under similar conditions (Almeida et al., 2013; Kürten et al., 2018). Figure 9 shows experimental and theoretical particle formation rates at vapor concentrations of  $[D]=3-140 \text{ ppt}_v$  and  $[N]=10-15 \text{ ppt}_v$ . In the simulations, the generic ion production rate is set to  $3 \text{ cm}^{-3} \text{ s}^{-1}$  and the ion-wall loss enhancement factor to 3.3. (see Almeida et al. (2013)).

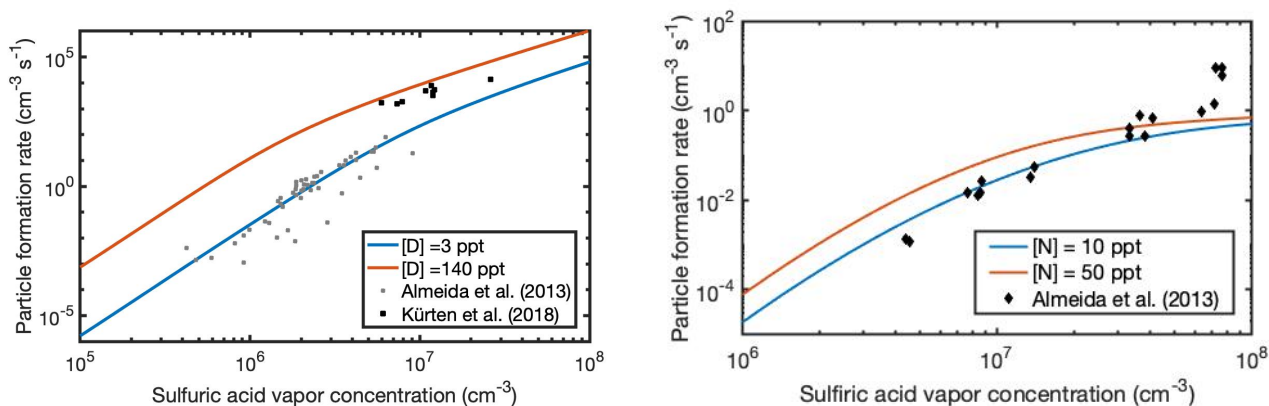


**Figure 9.** Particle formation rates observed at the CLOUD4 chamber experiment (markers) as a function of sulfuric acid vapor concentration at  $[D]=3\text{--}140\text{ ppt}_v$  (left) and  $[N]=10\text{--}50\text{ ppt}_v$  (right), and ACDC simulation results for particle formation in the presence of ions (lines). Note the different scales of  $x$  and  $y$  axes.

Figure 9 shows that the agreement between simulated and measured rates is good for both dimethylamine- and ammonia-containing clusters. In the case of dimethylamine, the measured data points from the study of Almeida et al. (2013) are close to the simulated  $[D]=3\text{ ppt}_v$  particle formation rate. However, recently Kürten et al. (2018) reanalyzed that data using a more advanced method. The reanalysis yielded an order of magnitude higher particle formation rates than previously assessed, and the reevaluated particle formation rates show a good agreement with our upper limit simulations  $[D]=140\text{ ppt}_v$ . For ammonia some experimental data points are ca. an order of magnitude higher than the simulated NPF rates, due to the plateauing of the simulated rates. This might be related to the effect of water in the experiments, as hydration is not considered in the present simulations. It has been shown that the effect of hydration is larger for clusters containing ammonia than for those containing dimethylamine. This is due to structural effects, such as the number of available hydrogen bond donors and acceptors within the cluster (Yang et al., 2018).

There are no measured particle formation data for guanidine, however, the good agreement between the simulations and experiments for dimethylamine and ammonia indicates that also the simulations for guanidine can be considered reliable. Figure 10 shows the NPF rates for  $[G]=0.001\text{--}10\text{ ppt}_v$  in the presence of ions with the same simulation conditions as for Figure 9, as well as a comparison to ion-free simulations for all the studied bases using the base concentration of  $1\text{ ppt}_v$ .

For guanidine, the enhancing effect of ions on the NPF rate is very small. This is due the fact that the electrically neutral clusters are already so stable that further stabilization by ionic molecules does not have a significant effect. In the case of dimethylamine, the presence of ions increases the NPF rate by up to an order of magnitude at low acid concentrations (although at these conditions even the increased NPF rate is atmospherically very low). For ammonia, the effect of ions is crucial, leading to up to 20 orders of magnitude increase in the NPF rate. This is largely due to the generation of neutral cluster formation by small ion cluster recombination, which allows clusters to "jump" over the unstable neutral cluster combinations. Since the thermodynamic barriers for anionic and cationic cluster growth are significantly lower compared to the neutral ammonia–sulfuric

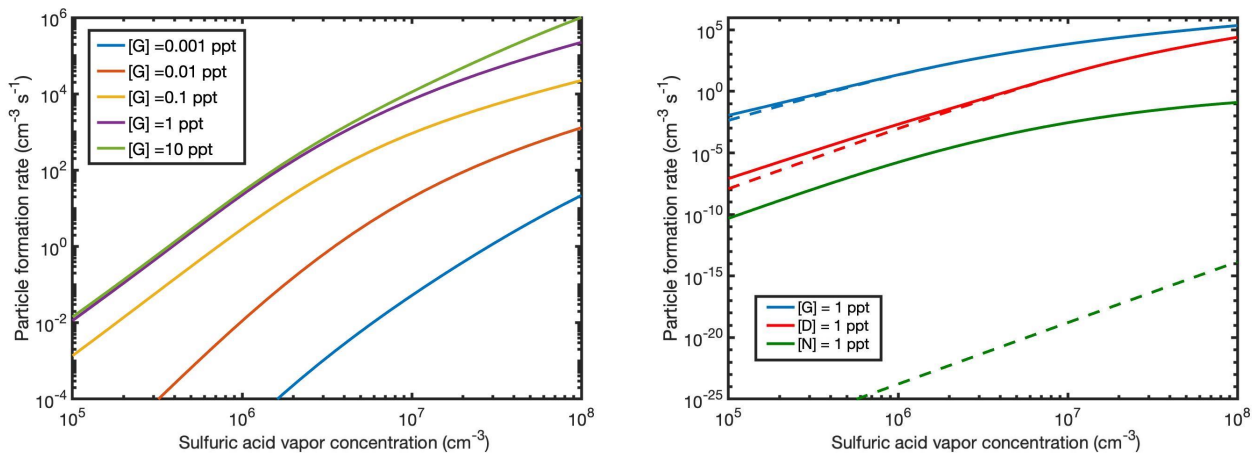


**Figure 10.** Particle formation rates from sulfuric acid and guanidine at  $[\text{guanidine}] = 0.001\text{--}10 \text{ ppt}_v$  in the presence of ions (left), and ion-mediated (solid line) and neutral (dashed line) particle formation rates for guanidine, dimethylamine and ammonia at base concentrations of  $1 \text{ ppt}_v$  (right) as a function of sulfuric acid vapor concentration.

acid case, larger clusters can form via collisions of medium-sized positively- and negatively-charged clusters. It should be noted that throughout the paper we have focused on *thermodynamic barriers*. In addition, the cluster growth might be hindered due to *kinetic barriers*. The addition of a monomer or a cluster to a pre-existing cluster might require cluster reorientation which in turn may lead to the breaking of intermolecular bonds, and thus, non-negligible kinetic barriers (DePalma et al., 2014; Bzdek et al., 2017; Xu et al., 2017). Thus, especially in the case of strongly-bound cage-like clusters, the subsequent growth as well as the evaporation may be slower than our calculations assume. For steady-state particle formation, however, the role of kinetic barriers is reduced assuming that the cluster formation and decomposition rate coefficients are connected by detailed balance. Because of this and for the fact that investigating all the possible barriers for formation and decomposition reactions is computationally very demanding, the kinetic barriers are neglected in this study.

### 3.6 Time-Dependent Simulations

It must be noted, however, that the total number of formed particles in a given time at atmospheric conditions is affected also by the time-dependent vapor concentrations. It is normally assumed that molecular clusters are a negligible sink of vapors, and that the concentration of vapor available for particle formation is determined by the vapor sources and the condensation sink onto larger particles. However, in the case of strongly clustering species and suppressed cluster evaporation, small clusters may take up a notable fraction of the vapor, leading to a negative feedback on particle formation due to vapor depletion. Therefore, in the atmosphere the particle formation efficiency of strong bases may be reduced compared to the steady-state predictions corresponding to constant vapor concentrations (Figures 10 and S2).

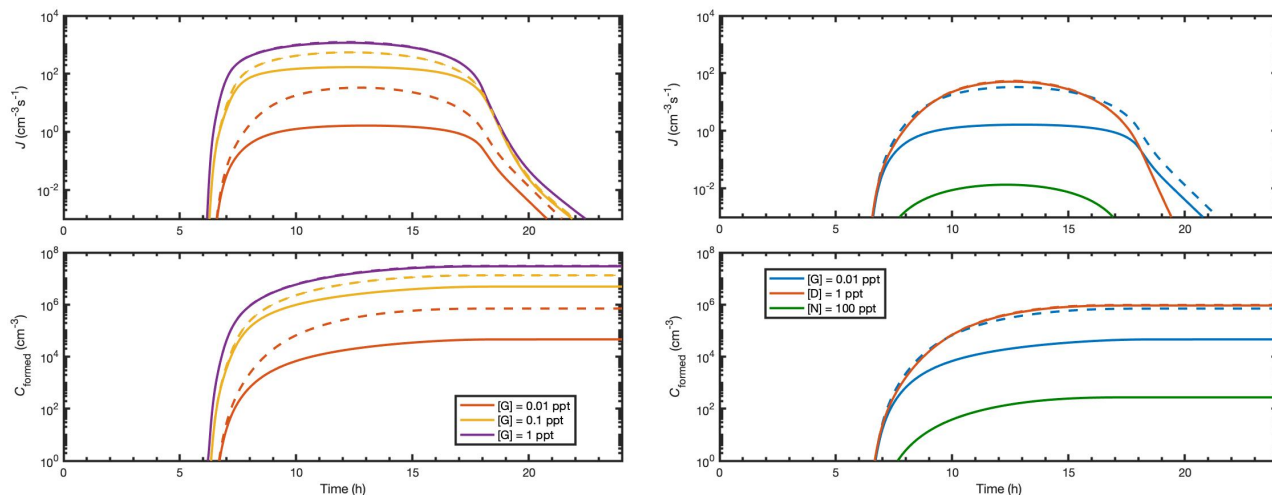


**Figure 11.** Particle formation rate  $J$  and concentration  $C_{\text{formed}}$  of formed particles as a function of time when either the base source is constant (solid lines) or the base concentration is constant (dashed lines).

Figure 11 demonstrates the effect of base vapor reduction due to clustering during a diurnal cycle where the source of sulfuric acid vapor is set to follow a sinusoidal function, mimicking atmospheric production of  $\text{H}_2\text{SO}_4$  from  $\text{SO}_2$  due to sunlight, and other parameters are set as in Figure S2. Dashed lines show the time-dependent particle formation rate (upper panels) and the total number of formed particles (lower panels) for simulations including both neutral and ionic clusters at a constant base concentration. Solid lines show results for a constant base source  $Q_{\text{base}} = L_{\text{base}} \times [\text{base}]$  that corresponds to the constant base concentrations assuming that they are determined solely by the source and the condensation sink  $L_{\text{base}}$ . For ammonia and dimethylamine, small clusters do not act as a notable sink to vapors, and the dashed and solid lines are indistinguishable from each other (right-hand side panels). For guanidine, however, a significant fraction of vapors can be bound to clusters, and neglecting this sink leads up to 1–2 orders of magnitude overprediction in the concentrations of formed particles (dashed vs. solid lines in the lower panels). This effect is particularly significant at low vapor levels, but becomes negligible at a higher guanidine concentration or source (lines with different colors in the left-hand side panels).

While the effects depicted in Figure 11 do not affect steady-state particle formation investigations, such as the CLOUD set-up, they should be considered in the interpretation of field measurements and predictions of ambient aerosol formation, if there is reason to believe that strongly clustering species may be present and their sources can be assessed. Time-dependent clustering simulations can be embedded in, for instance, an atmospheric box model to probe the vapor–cluster exchange dynamics. Such modeling approach can be applied to interpret field observations, and to estimate the vapor sink caused by clustering at different conditions.

## 4 Conclusions

We have investigated the enhancing potential of weak (ammonia), medium strong (dimethylamine) and very strong (guanidine) bases in atmospheric particle formation. In the studied sulfuric acid–base systems, molecular cluster growth proceeds through "diagonal" cluster compositions that contain approximately equal numbers of acid and base molecules. However, the difference between dimethylamine or ammonia and guanidine is that the growth of clusters containing the relatively weaker bases occurs via monomeric acid and base additions, whereas guanidine clusters mainly grow via acid–base heterodimer additions. This is because guanidine and sulfuric acid can form a complex with an evaporation rate as low as  $10^{-5} \text{ s}^{-1}$ , meaning that the probability for the complex to collide with an other heterodimer or a larger cluster is much higher than its probability to evaporate. We studied the structures of the diagonal clusters and showed that guanidine and sulfuric acid form extremely stable mesh-like cluster structures, which have a high symmetry and a large number of strong intermolecular interactions between bisulfate and guanidinium while the hydroxyl groups of the bisulfates remain free. Dimethylamine and ammonia form less symmetric structures with sulfuric acid, and the hydroxyl groups of the bisulfates form intermolecular interactions with each other. It is clear that the interaction between a bisulfate and a protonated base is much stronger than that between two bisulfates, and thus, the intermolecular interactions in the dimethylamine and ammonia clusters are much weaker than those in the guanidine clusters. By using relative base concentrations calculated from mass-balance relation, corresponding to the same equilibrium concentration for different heterodimers, we showed that the enhancing potential of a base is largely dominated by the intermolecular interactions between the acid and base molecules, and the atmospheric abundance of the base plays only a minor role in terms of cluster stability. Due to the fact that unprotonated guanidine is a semi-volatile compound, its actual atmospheric concentration may be much higher than the values used in this theoretical study. Also other strong base compounds, such as amidines and guanidine derivatives, are likely to have a higher enhancing potential in particle formation compared to medium strong bases such as alkylamines.

We compared simulated particle formation rates, based on the calculated Gibbs free energies, to rates measured in field and laboratory studies and found a good agreement for sulfuric acid–ammonia and sulfuric acid–dimethylamine particle formation. In addition, we compared simulated NPF rates with or without ions for the three representative bases, and demonstrated that in ion-mediated particle formation, the role of base strength is much smaller than in electrically neutral cases. In the case of ammonia, the enhancing effect of ions is significant, increasing the NPF rates by up to 20 orders of magnitude. For ammonia, the main neutral cluster growth pathway contains unstable clusters with evaporation rates up to  $10^5 \text{ s}^{-1}$ , whereas the growth by formation of smaller anionic and cationic clusters and their subsequent recombination to larger neutral clusters occurs via stable clusters with much lower evaporation rates. In the case of guanidine, electrically neutral clusters are already tightly bound, and therefore, the effect of ions is very small.

Under atmospheric conditions, both ammonia and dimethylamine can be available, and new-particle formation may occur via three-component pathways. This three-component pathway can lead to higher new-particle formation rates than the two-component pathways for two main reasons: 1) base exchange and 2) synergistic effects. 1) For pre-existing sulfuric acid–ammonia clusters, the substitution of ammonia by dimethylamine can be assumed to be fast based on studies by e.g. Bzdek

et al. (2017) and Kupiainen et al. (2012). 2) When sulfuric acid–dimethylamine clusters uptake ammonia molecules, the number of intermolecular bonds increases which can further stabilize the clusters and thus make the subsequent cluster growth faster, as we have showed recently (Myllys et al., 2019). The role of base exchange and synergy are yet unresolved in the case of guanidine; however, since guanidine is a stronger base and capable of forming more intermolecular bonds than ammonia or dimethylamine, the reasonable assumption would be that guanidine can replace either ammonia or dimethylamine fast and that the replacement increases the cluster stability and particle formation rate. As sulfuric acid and guanidine form very stable clusters containing a large number of intermolecular bonds, we do not expect that the presence of either ammonia or dimethylamine would enhance the particle formation by synergistic effects.

Due to the substantial computational effort required, water is not included in the cluster structures or particle formation simulations of this study. It has been demonstrated that the enhancing effect of hydration is larger in the case of ammonia than dimethylamine (Olenius et al., 2017), and the reason is likely to be the number of available hydrogen bonds in the cluster structure (Yang et al., 2018). While the effect of water on guanidine–sulfuric acid particle formation remains to be resolved, the possible enhancement can be expected to be small as the unhydrated clusters are already extremely stable. Our study shows that the role of base strength and cluster structure, which affect the number and strength of intermolecular interactions, are often more important than differences in the typical atmospheric concentrations of different bases for steady-state particle formation. Therefore, when investigating the importance of acid–base chemistry on the formation and properties of atmospheric aerosol particles, impacts of strong organobases with very low concentrations should be included. The atmosphere is a complex mixture containing various potential contributors to NPF and identifying all the most relevant compounds and investigating their particle formation efficiency at different relative humidities is mandatory in order to understand and predict the importance of acid–base NPF in different atmospheric environments.

*Author contributions.* The study design, most of the calculations and simulations, and manuscript preparation were performed by NM. New configurational sampling were performed by JK and VB, experiments were performed and analyzed by DA and MP, time-dependent simulations were performed and analyzed by TO, and insightful discussion followed by valuable suggestions were given by JS. All co-authors proofread and commented the manuscript.

25 *Competing interests.* The authors declare that they have no conflict of interests.

*Acknowledgements.* We thank the Academy of Finland and ERC project 692891-DAMOCLES for funding, and the CSC-IT Center for Science in Espoo, Finland, for computational resources. NM thanks the Jenny and Antti Wihuri foundation for financial support. JS acknowledges funding from the U.S. National Science Foundation under grant no. CHE-1710580. TO thanks the ÅForsk foundation (project 18-334) and the Knut and Alice Wallenberg foundation (Academy Fellowship AtmoRemove) for funding. We thank professor R.B. Gerber for helpful discussion and doctor A. Kürten for valuable suggestion to use the reevaluated CLOUD data.

## References

- Ahlm, L., Yli-Juuti, T., Schobesberger, S., Praplan, A. P., Kim, J., Tikkanen, O.-P., Lawler, M. J., Smith, J. N., Tröstl, J., Navarro, J. C. A., Baltensperger, U., Bianchi, F., Donahue, N. M., Duplissy, J., Franchin, A., Jokinen, T., Keskinen, H., Kirkby, J., Kürten, A., Laaksonen, A., Lehtipalo, K., Petäjä, T., Riccobono, F., Rissanen, M. P., Rondo, L., Schallhart, S., Simon, M., Winkler, P. M., Worsnop, D. R., Virtanen, A., and Riipinen, I.: Modeling the thermodynamics and kinetics of sulfuric acid-dimethylamine-water nanoparticle growth in the CLOUD chamber, *Aerosol Sci. Tech.*, 50, 1017–1032, <https://doi.org/10.1080/02786826.2016.1223268>, 2016.
- Almeida, J., Schobesberger, S., Kürten, A., Ortega, I. K., Kupiainen-Määttä, O., Praplan, A. P., Adamov, A., Amorim, A., Bianchi, F., Breitenlechner, M., and *et al.*: Molecular Understanding of Sulphuric Acid–Amine Particle Nucleation in the Atmosphere, *Nature*, 502, 359–363, 2013.
- Anderson, N., Strader, R., and Davidson, C.: Airborne Reduced Nitrogen: Ammonia Emissions from Agriculture and Other Sources, *Environ. Int.*, 29, 277–286, 2003.
- Angyal, S. J. and Warburton, W. K.: The Basic Strengths of Methylated Guanidines, *J. Chem. Soc.*, 549, 2492–2494, <https://doi.org/10.1039/JR9510002492>, <http://dx.doi.org/10.1039/JR9510002492>, 1951.
- Bonas, J. E., Cohen, B. D., and Natelson, S.: Separation and Estimation of Certain Guanidino Compounds. Application to Human Urine, *Microchem. J.*, 7, 63–77, [https://doi.org/http://dx.doi.org/10.1016/0026-265X\(63\)90012-2](https://doi.org/http://dx.doi.org/10.1016/0026-265X(63)90012-2), <http://www.sciencedirect.com/science/article/pii/0026265X63900122>, 1963.
- Bzdek, B. R., DePalma, J. W., and Johnston, M. V.: Mechanisms of Atmospherically Relevant Cluster Growth, *Acc. Chem. Res.*, 50, 1965–1975, <https://doi.org/10.1021/acs.accounts.7b00213>, 2017.
- Chai, J.-D. and Head-Gordon, M.: Long-Range Corrected Hybrid Density Functionals with Damped Atom-Atom Dispersion Corrections, *Phys. Chem. Chem. Phys.*, 10, 6615–6620, <https://doi.org/10.1039/B810189B>, <http://dx.doi.org/10.1039/B810189B>, 2008.
- DePalma, J. W., Bzdek, B. R., Ridge, D. P., and Johnston, M. V.: Activation Barriers in the Growth of Molecular Clusters Derived from Sulfuric Acid and Ammonia, *The Journal of Physical Chemistry A*, 118, 11 547–11 554, <https://doi.org/10.1021/jp507769b>, 2014.
- Elm, J.: Elucidating the Limiting Steps in Sulfuric Acid–Base New Particle Formation, *J. Phys. Chem. A*, 121, 8288–8295, <https://doi.org/10.1021/acs.jpca.7b08962>, 2017.
- Elm, J., Jen, C. N., Kurtén, T., and Vehkamäki, H.: Strong Hydrogen Bonded Molecular Interactions between Atmospheric Diamines and Sulfuric Acid, *J. Phys. Chem. A*, 120, 3693–3700, <https://doi.org/10.1021/acs.jpca.6b03192>, 2016.
- Elm, J., Passananti, M., Kurtén, T., and Vehkamäki, H.: Diamines Can Initiate New Particle Formation in the Atmosphere, *J. Phys. Chem. A*, 121, 6155–6164, <https://doi.org/10.1021/acs.jpca.7b05658>, 2017.
- Frisch, M. J., Trucks, G. W., Schlegel, H. B., Scuseria, G. E., Robb, M. A., Cheeseman, J. R., Scalmani, G., Barone, V., Petersson, G. A., Nakatsuji, H., Li, X., Caricato, M., Marenich, A. V., Bloino, J., Janesko, B. G., Gomperts, R., Mennucci, B., Hratchian, H. P., Ortiz, J. V., Izmaylov, A. F., Sonnenberg, J. L., Williams-Young, D., Ding, F., Lipparini, F., Egidi, F., Goings, J., Peng, B., Petrone, A., Henderson, T., Ranasinghe, D., Zakrzewski, V. G., Gao, J., Rega, N., Zheng, G., Liang, W., Hada, M., Ehara, M., Toyota, K., Fukuda, R., Hasegawa, J., Ishida, M., Nakajima, T., Honda, Y., Kitao, O., Nakai, H., Vreven, T., Throssell, K., Montgomery, Jr., J. A., Peralta, J. E., Ogliaro, F., Bearpark, M. J., Heyd, J. J., Brothers, E. N., Kudin, K. N., Staroverov, V. N., Keith, T. A., Kobayashi, R., Normand, J., Raghavachari, K., Rendell, A. P., Burant, J. C., Iyengar, S. S., Tomasi, J., Cossi, M., Millam, J. M., Klene, M., Adamo, C., Cammi, R., Ochterski, J. W., Martin, R. L., Morokuma, K., Farkas, O., Foresman, J. B., and Fox, D. J.: Gaussian16 Revision A.03, 2016.

- Ge, X., Wexler, A. S., and Clegg, S. L.: Atmospheric Amines – Part I. A Review, *Atmos. Environ.*, 45, 524–546, <https://doi.org/http://dx.doi.org/10.1016/j.atmosenv.2010.10.012>, <http://www.Sciencedirect.com/Science/article/pii/S1352231010008745>, 2011.
- 5 Glasoe, W., Volz, K., Panta, B., Freshour, N., Bachman, R., Hanson, D., McMurry, P., and Jen, C.: Sulfuric Acid Nucleation: An Experimental Study of the Effect of Seven Bases, *J. Geophys. Res. Atmos.*, 120, 1933–1950, 2015.
- Hallquist, M., Wenger, J. C., Baltensperger, U., Rudich, Y., Simpson, D., Claeys, M., Dommen, J., Donahue, N. M., George, C., Goldstein, A. H., Hamilton, J. F., Herrmann, H., Hoffmann, T., Iinuma, Y., Jang, M., Jenkin, M. E., Jimenez, J. L., Kiendler-Scharr, A., Maenhaut, W., McFiggans, G., Mentel, T. F., Monod, A., Prévôt, A. S. H., Seinfeld, J. H., Surratt, J. D., Szmigielski, R., and Wildt, J.: The Formation, Properties and Impact of Secondary Organic Aerosol: Current and Emerging Issues, *Atmos. Chem. Phys.*, 9, 5155–5236, <https://doi.org/10.5194/acp-9-5155-2009>, <https://www.atmos-chem-phys.net/9/5155/2009/>, 2009.
- 10 Heinritzi, M., Simon, M., Steiner, G., Wagner, A. C., Kürten, A., Hansel, A., and Curtius, J.: Characterization of the Mass-Dependent Transmission Efficiency of a CIMS, *Atmos. Meas. Tech.*, 9, 1449–1460, <https://doi.org/10.5194/amt-9-1449-2016>, <https://www.atmos-meas-tech.net/9/1449/2016/>, 2016.
- Ho, K.-L., Chung, Y.-C., Lin, Y.-H., and Tseng, C.-P.: Biofiltration of Trimethylamine, Dimethylamine, and Methylamine by Immobilized Paracoccus sp. CP2 and Arthrobacter sp. CP1, *Chemosphere*, 72, 250–256, 2008.
- 15 Jen, C. N., Bachman, R., Zhao, J., McMurry, P. H., and Hanson, D. R.: Diamine-Sulfuric Acid Reactions Are a Potent Source of New Particle Formation, *Geophys. Res. Lett.*, 43, 867–873, <https://doi.org/10.1002/2015GL066958>, <http://dx.doi.org/10.1002/2015GL066958>, 2016.
- Junninen, H., Ehn, M., Petäjä, T., Luosujärvi, L., Kotiaho, T., Kostianen, R., Rohner, U., Gonin, M., Fuhrer, K., Kulmala, M., and Worsnop, D. R.: A High-Resolution Mass Spectrometer to Measure Atmospheric Ion Composition, *Atmos. Meas. Tech.*, 3, 1039–1053, <https://doi.org/10.5194/amt-3-1039-2010>, <https://www.atmos-meas-tech.net/3/1039/2010/>, 2010.
- 20 Kaplan, D. L., Cornell, J. H., and Kaplan, A. M.: Decomposition of Nitroguanidine, *Environ. Sci. Tech.*, 16, 488–492, 1982.
- Kendall, R. A., Dunning, T. H., and Harrison, R. J.: Electron Affinities of the First-Row Atoms Revisited. Systematic Basis Sets and Wave Functions, *J. Chem. Phys.*, 96, 6796–6806, <https://doi.org/http://dx.doi.org/10.1063/1.462569>, <http://scitation.aip.org/content/aip/journal/jcp/96/9/10.1063/1.462569>, 1992.
- 25 Kirkby, J., Duplissy, J., Sengupta, K., Frege, C., Gordon, H., Williamson, C., Heinritzi, M., Simon, M., Yan, C., Almeida, J., Trostl, J., Nieminen, T., Ortega, I., Wagner, R., Adamov, A., Amorim, A., Bernhammer, A.-K., Bianchi, F., Breitenlechner, M., Brilke, S., Chen, X., Craven, J., Dias, A., Ehrhart, S., Flagan, R., Franchin, A., Fuchs, C., Guida, R., Hakala, J., Hoyle, C., Jokinen, T., Junninen, H., Kangasluoma, J., Kim, J., Krapf, M., Kurtén, A., Laaksonen, A., Lehtipalo, K., Makhmutov, V., Mathot, S., Molteni, U., Onnela, A., Perakyla, O., Piel, F., Petaja, T., Praplan, A., Pringle, K., Rap, A., Richards, N., Riipinen, I., Rissanen, M., Rondo, L., Sarnela, N., Schobesberger, S., Scott, C., Seinfeld, J., Sipila, M., Steiner, G., Stozhkov, Y., Stratmann, F., Tomić, A., Virtanen, A., Vogel, A., Wagner, A., Wagner, P., Weingartner, E., Wimmer, D., Winkler, P., Ye, P., Zhang, X., Hansel, A., Dommen, J., Donahue, N., Worsnop, D., Baltensperger, U., Kulmala, M., Carslaw, K., and Curtius, J.: Ion-Induced Nucleation of Pure Biogenic Particles, *Nature*, 533, 521–526, <https://doi.org/10.1038/nature17953>, 2016.
- 30 Krishnan, R., Binkley, J. S., Seeger, R., and Pople, J. A.: Self-Consistent Molecular Orbital Methods. XX. A Basis Set for Correlated Wave Functions, *J. Chem. Phys.*, 72, 650–654, <https://doi.org/http://dx.doi.org/10.1063/1.438955>, <http://scitation.aip.org/content/aip/journal/jcp/72/1/10.1063/1.438955>, 1980.

- Kulmala, M., Riipinen, I., Sipilä, M., Manninen, H. E., Petäjä, T., Junninen, H., Maso, M. D., Mordas, G., Mirme, A., Vana, M., Hirsikko, A., Laakso, L., Harrison, R. M., Hanson, I., Leung, C., Lehtinen, K. E. J., and Kerminen, V.-M.: Toward Direct Measurement of Atmospheric Nucleation, *Science*, 318, 89–92, <https://doi.org/10.1126/science.1144124>, <http://science.sciencemag.org/content/318/5847/89>, 2007.
- 5 Kulmala, M., Kontkanen, J., Junninen, H., Lehtipalo, K., Manninen, H. E., Nieminen, T., Petäjä, T., Sipilä, M., Schobesberger, S., Rantala, P., Franchin, A., Jokinen, T., Järvinen, E., Äijälä, M., Kangasluoma, J., Hakala, J., Aalto, P. P., Paasonen, P., Mikkilä, J., Vanhanen, J., Aalto, J., Hakola, H., Makkonen, U., Ruuskanen, T., Mauldin, R. L., Duplissy, J., Vehkamäki, H., Bäck, J., Kortelainen, A., Riipinen, I., Kurtén, T., Johnston, M. V., Smith, J. N., Ehn, M., Mentel, T. F., Lehtinen, K. E. J., Laaksonen, A., Kerminen, V.-M., and Worsnop, D. R.: Direct Observations of Atmospheric Aerosol Nucleation, *Science*, 339, 943–946, <https://doi.org/10.1126/science.1227385>, <http://science.sciencemag.org/content/339/6122/943>, 2013.
- 10 Kumar, R., Choudhary, V., Mishra, S., Varma, I., and Mattiason, B.: Adhesives and Plastics Based on Soy Protein Products, *Ind. Crops Prod.*, 16, 155–172, [https://doi.org/http://dx.doi.org/10.1016/S0926-6690\(02\)00007-9](https://doi.org/http://dx.doi.org/10.1016/S0926-6690(02)00007-9), <http://www.sciencedirect.com/science/article/pii/S0926669002000079>, 2002.
- Kupiainen, O., Ortega, I. K., Kurtén, T., and Vehkamäki, H.: Amine Substitution into Sulfuric Acid–Ammonia Clusters, *Atmos. Chem. Phys.*, 12, 3591–3599, 2012.
- 15 Kürten, A., Li, C., Bianchi, F., Curtius, J., Dias, A., Donahue, N. M., Duplissy, J., Flagan, R. C., Hakala, J., Jokinen, T., Kirkby, J., Kulmala, M., Laaksonen, A., Lehtipalo, K., Makhmutov, V., Onnela, A., Rissanen, M. P., Simon, M., Sipilä, M., Stozhkov, Y., Tröstl, J., Ye, P., and McMurry, P. H.: New Particle Formation in the Sulfuric Acid–Dimethylamine–Water System: Reevaluation of CLOUD Chamber Measurements and Comparison to an Aerosol Nucleation and Growth Model, *Atmos. Chem. Phys.*, 18, 845–863, <https://doi.org/10.5194/acp-18-845-2018>, <https://www.atmos-chem-phys.net/18/845/2018/>, 2018.
- 20 Kurtén, T., Torpo, L., Ding, C.-G., Vehkamäki, H., Sundberg, M. R., Laasonen, K., and Kulmala, M.: A Density Functional Study on Water-Sulfuric Acid–Ammonia Clusters and Implications for Atmospheric Cluster Formation, *J. Geophys. Res. Atmos.*, 112, D04 210, <https://doi.org/10.1029/2006JD007391>, <http://dx.doi.org/10.1029/2006JD007391>, 2007.
- Kurtén, T., Loukonen, V., Vehkamäki, H., and Kulmala, M.: Amines Are Likely to Enhance Neutral and Ion-Induced Sulfuric Acid–Water Nucleation in the Atmosphere More Effectively Than Ammonia, *Atmos. Chem. Phys.*, 8, 4095–4103, <https://doi.org/10.5194/acp-8-4095-2008>, <https://www.atmos-chem-phys.net/8/4095/2008/>, 2008.
- 25 Lehtipalo, K., Rondo, L., Kontkanen, J., Schobesberger, S., Jokinen, T., Sarnela, N., Kürten, A., Ehrhart, S., Franchin, A., Nieminen, T., et al.: The Effect of Acid–Base Clustering and Ions on the Growth of Atmospheric Nano-Particles, *Nature Comm.*, 7, 11 594, 2016.
- Liakos, D. G., Sparta, M., Kesharwani, M. K., Martin, J. M. L., and Neese, F.: Exploring the Accuracy Limits of Local Pair Natural Orbital Coupled-Cluster Theory, *J. Chem. Theory Comput.*, 11, 1525–1539, <https://doi.org/10.1021/ct501129s>, 2015.
- 30 Marescau, B., Deshmukh, D. R., Kockx, M., Possemiers, I., Qureshi, I. A., Wiechert, P., and Deyn, P. P. D.: Guanidino Compounds in Serum, Urine, Liver, Kidney, and Brain of Man and Some Ureotelic Animals, *Metabolism*, 41, 526–532, [https://doi.org/http://dx.doi.org/10.1016/0026-0495\(92\)90213-T](https://doi.org/http://dx.doi.org/10.1016/0026-0495(92)90213-T), <http://www.sciencedirect.com/science/article/pii/002604959290213T>, 1992.
- McGrath, M. J., Olenius, T., Ortega, I. K., Loukonen, V., Paasonen, P., Kurtén, T., Kulmala, M., and Vehkamäki, H.: Atmospheric Cluster Dynamics Code: a Flexible Method for Solution of the Birth–Death Equations, *Atmos. Chem. Phys.*, 12, 2345–2355, <https://doi.org/10.5194/acp-12-2345-2012>, <http://www.atmos-chem-phys.net/12/2345/2012/>, 2012.
- Myllys, N.: From Electronic Structures to Molecular-Level Cluster Formation Mechanisms in the Atmosphere, Ph.D. thesis, University of Helsinki, Finland, 2017.

- Myllys, N., Elm, J., Halonen, R., Kurtén, T., and Vehkamäki, H.: Coupled Cluster Evaluation of the Stability of Atmospheric Acid–Base Clusters with up to 10 Molecules, *J. Phys. Chem. A*, 120, 621–630, <https://doi.org/10.1021/acs.jpca.5b09762>, 2016a.
- Myllys, N., Elm, J., and Kurtén, T.: Density Functional Theory Basis Set Convergence of Sulfuric Acid-Containing Molecular Clusters, *Comput. Theor. Chem.*, 1098, 1–12, <https://doi.org/http://dx.doi.org/10.1016/j.comptc.2016.10.015>, <http://www.sciencedirect.com/science/article/pii/S2210271X16304297>, 2016b.
- 5 Myllys, N., Ponkkonen, T., Passananti, M., Elm, J., Vehkamäki, H., and Olenius, T.: Guanidine: A Highly Efficient Stabilizer in Atmospheric New-Particle Formation, *J. Phys. Chem. A*, 122, 4717–4729, <https://doi.org/10.1021/acs.jpca.8b02507>, 2018.
- Myllys, N., Chee, S., Olenius, T., Lawler, M., and Smith, J. N.: Molecular-Level Understanding of Synergistic Effects in Sulfuric Acid–Amine–Ammonia Mixed Clusters, *J. Phys. Chem. A*, 123, 2420–2425, <https://doi.org/10.1021/acs.jpca.9b00909>, 2019.
- 10 Neese, F.: The ORCA Program System, *Wiley Interdiscip. Rev. Comput. Mol. Sci.*, 2, 73–78, <https://doi.org/10.1002/wcms.81>, <http://dx.doi.org/10.1002/wcms.81>, 2012.
- Olenius, T., Kupiainen-Määttä, O., Ortega, I. K., Kurtén, T., and Vehkamäki, H.: Free Energy Barrier in the Growth of Sulfuric Acid–Ammonia and Sulfuric Acid–Dimethylamine Clusters, *J. Chem. Phys.*, 139, 084312, <https://doi.org/http://dx.doi.org/10.1063/1.4819024>, <http://scitation.aip.org/content/aip/journal/jcp/139/8/10.1063/1.4819024>, 2013.
- 15 Olenius, T., Halonen, R., Kurtén, T., Henschel, H., Kupiainen-Määttä, O., Ortega, I. K., Jen, C. N., Vehkamäki, H., and Riipinen, I.: New Particle Formation from Sulfuric Acid and Amines: Comparison of Mono-, Di-, and Trimethylamines, *J. Geophys. Res. Atmos.*, 122, 7103–7118, <https://doi.org/10.1002/2017JD026501>, <http://dx.doi.org/10.1002/2017JD026501>, 2017.
- Oxley, J. C., Smith, J. L., Naik, S., and Moran, J.: Decompositions of Urea and Guanidine Nitrates, *J. Energ. Mater.*, 27, 17–39, <https://doi.org/10.1080/07370650802328814>, 2008.
- 20 Riplinger, C. and Neese, F.: An Efficient and Near Linear Scaling Pair Natural Orbital Based Local Coupled Cluster Method, *J. Chem. Phys.*, 138, 034106, <https://doi.org/http://dx.doi.org/10.1063/1.4773581>, <http://scitation.aip.org/content/aip/journal/jcp/138/3/10.1063/1.4773581>, 2013.
- Riplinger, C., Sandhoefer, B., Hansen, A., and Neese, F.: Natural Triple Excitations in Local Coupled Cluster Calculations with Pair Natural Orbitals, *J. Chem. Phys.*, 139, 134101, <https://doi.org/http://dx.doi.org/10.1063/1.4821834>, <http://scitation.aip.org/content/aip/journal/jcp/139/13/10.1063/1.4821834>, 2013.
- 25 Riplinger, C., Pinski, P., Becker, U., Valeev, E. F., and Neese, F.: Sparse Maps—A Systematic Infrastructure for Reduced-Scaling Electronic Structure Methods. II. Linear Scaling Domain Based Pair Natural Orbital Coupled Cluster Theory, *J. Chem. Phys.*, 144, 024 109, <https://doi.org/10.1063/1.4939030>, 2016.
- Swick, R. W.: Measurement of Protein Turnover in Rat Liver., *J. Biol. Chem.*, 231, 751–764, 1958.
- 30 Temelso, B., Morrison, E. F., Speer, D. L., Cao, B. C., Appiah-Padi, N., Kim, G., and Shields, G. C.: Effect of Mixing Ammonia and Alkylamines on Sulfate Aerosol Formation, *J. Phys. Chem. A*, 122, 1612–1622, <https://doi.org/10.1021/acs.jpca.7b11236>, 2018.
- The Merck Index: An Encyclopedia of Chemicals, Drugs, and Biologicals, RSC Adv., 2013.
- Van Pilsum, J. F., Martin, R. P., Kito, E., and Hess, J.: Determination of Creatine, Creatinine, Arginine, Guanidinoacetic Acid, Guanidine, and Methylguanidine in Biological Fluids., *J. Biol. Chem.*, 222, 225–236, 1956.
- 35 Wagner, R., Yan, C., Lehtipalo, K., Duplissy, J., Nieminen, T., Kangasluoma, J., Ahonen, L. R., Dada, L., Kontkanen, J., Manninen, H. E., Dias, A., Amorim, A., Bauer, P. S., Bergen, A., Bernhammer, A.-K., Bianchi, F., Brilke, S., Mazon, S. B., Chen, X., Draper, D. C., Fischer, L., Frege, C., Fuchs, C., Garmash, O., Gordon, H., Hakala, J., Heikkinen, L., Heinritzi, M., Hofbauer, V., Hoyle, C. R., Kirkby, J., Kürten, A., Kvashnin, A. N., Laurila, T., Lawler, M. J., Mai, H., Makhmutov, V., Mauldin III, R. L., Molteni, U., Nichman, L., Nie, W.,

- Ojdanic, A., Onnela, A., Piel, F., Quéléver, L. L. J., Rissanen, M. P., Sarnela, N., Schallhart, S., Sengupta, K., Simon, M., Stolzenburg, D., Stozhkov, Y., Tröstl, J., Viisanen, Y., Vogel, A. L., Wagner, A. C., Xiao, M., Ye, P., Baltensperger, U., Curtius, J., Donahue, N. M., Flagan, R. C., Gallagher, M., Hansel, A., Smith, J. N., Tomé, A., Winkler, P. M., Worsnop, D., Ehn, M., Sipilä, M., Kerminen, V.-M., Petäjä, T., and Kulmala, M.: The Role of Ions in New Particle Formation in the CLOUD Chamber, *Atmos. Chem. Phys.*, 17, 15 181–15 197, <https://doi.org/10.5194/acp-17-15181-2017>, <https://www.atmos-chem-phys.net/17/15181/2017/>, 2017.
- 5 Xie, H.-B., Elm, J., Halonen, R., Myllys, N., Kurtén, T., Kulmala, M., and Vehkamäki, H.: Atmospheric Fate of Monoethanolamine: Enhancing New Particle Formation of Sulfuric Acid as an Important Removal Process, *Environ. Sci. Technol.*, 51, 8422–8431, <https://doi.org/10.1021/acs.est.7b02294>, 2017.
- Xu, J., Finlayson-Pitts, B. J., and Gerber, R. B.: Nanoparticles Grown from Methanesulfonic Acid and Methylamine: Microscopic Structures and Formation Mechanism, *Phys. Chem. Chem. Phys.*, 19, 31 949–31 957, <https://doi.org/10.1039/C7CP06489F>, <http://dx.doi.org/10.1039/C7CP06489F>, 2017.
- 10 Yang, Y., Waller, S. E., Kreinbihl, J. J., and Johnson, C. J.: Direct Link between Structure and Hydration in Ammonium and Aminium Bisulfate Clusters Implicated in Atmospheric New Particle Formation, *J. Phys. Chem. Lett.*, 9, 5647–5652, <https://doi.org/10.1021/acs.jpcclett.8b02500>, 2018.
- 15 Yao, L., Garmash, O., Bianchi, F., Zheng, J., Yan, C., Kontkanen, J., Junninen, H., Mazon, S. B., Ehn, M., Paasonen, P., Sipilä, M., Wang, M., Wang, X., Xiao, S., Chen, H., Lu, Y., Zhang, B., Wang, D., Fu, Q., Geng, F., Li, L., Wang, H., Qiao, L., Yang, X., Chen, J., Kerminen, V.-M., Petäjä, T., Worsnop, D. R., Kulmala, M., and Wang, L.: Atmospheric New Particle Formation from Sulfuric Acid and Amines in a Chinese Megacity, *Science*, 361, 278–281, <https://doi.org/10.1126/science.aao4839>, <http://science.sciencemag.org/content/361/6399/278>, 2018.
- 20 Yu, H., McGraw, R., and Lee, S.-H.: Effects of Amines on Formation of Sub-3 nm Particles and Their Subsequent Growth, *Geophys. Res. Lett.*, 39, 2, 2012.
- Zhang, R., Khalizov, A., Wang, L., Hu, M., and Xu, W.: Nucleation and Growth of Nanoparticles in the Atmosphere, *Chem. Rev.*, 112, 1957–2011, <https://doi.org/10.1021/cr2001756>, 2012.
- Zhao, Z., Dai, Y., Ge, G., and Wang, G.: Guanidine Nitrate Enhanced Catalysis of Nitrogen-Doped Carbon Nanotubes for Metal-Free Styrene Production through Direct Dehydrogenation, *Chem. Cat. Chem.*, 7, 1135–1144, <https://doi.org/10.1002/cctc.201402934>, <http://dx.doi.org/10.1002/cctc.201402934>, 2015.
- 25

Supporting Information  
for  
Role of Base Strength, Cluster Structure and  
Charge in Sulfuric Acid-Driven Particle  
Formation

Nanna Myllys,<sup>\*,†,‡,||</sup> Jakub Kubečka,<sup>‡</sup> Vitus Besel,<sup>‡</sup> Dina Alfaouri,<sup>‡</sup> Tinja Olenius,<sup>¶</sup>  
James Smith,<sup>†</sup> and Monica Passananti<sup>§,‡</sup>

<sup>†</sup>*Department of Chemistry, University of California, Irvine*

<sup>‡</sup>*Institute for Atmospheric and Earth System Research, University of Helsinki*

<sup>¶</sup>*Department of Environmental Science and Analytical Chemistry & Bolin Centre for  
Climate Research, Stockholm University*

<sup>§</sup>*Dipartimento di Chimica, Università di Torino*

<sup>||</sup>*+358 503812141*

E-mail: [nanna.myllys@uci.edu](mailto:nanna.myllys@uci.edu)

## Cluster Structures and Gibbs Free Binding Energies

As stated in the main text, we have used cluster structures of our previous works as a base of our study.<sup>1-3</sup> For cluster structures not studied before, we have performed a new configurational sampling procedure, explained below. In addition, if some previously found cluster structures seemed to be outlying from the general trends, we have re-sampled them to find a better configuration.

First, we used a recently introduced genetic algorithm, the Artificial Bee Colony (ABC) algorithm,<sup>4</sup> to explore the Potential Energy Surface (PES) of the desired molecular cluster. We utilized the ABCcluster program,<sup>5,6</sup> which uses ABC to explore the PES of clusters composed of rigid molecular units. Assuming rigidity of molecules is no problem since the molecular clusters will be optimized in the further steps. Thus, assuming all possible combinations of molecular units (isomers and protonation states) we explored the PES on the Molecular Mechanics (MM) level with Force Field (FF) parameters taken from the CHARMM database.<sup>7,8</sup> We used the following ABCcluster specification: 2000 initial random guesses, 100 generations (exploration loops) and 5 scout bees, and saved 5000 energetically lowest-lying local minima for each combination of molecular units.

Second, all structures found by ABCcluster were re-optimized by the tight-binding semi-empirical program GFN-*x*TB with very tight optimization criteria.<sup>9</sup> Many of the structures relaxed to the same minimum on the PES. Thus, we removed all redundant structures based on the total GFN-*x*TB energy and the radius of gyration (a geometry property incorporating cluster size and mass distribution). Two structures were combined if the total GFN-*x*TB energy difference was lower than 0.001 Hartree and the gyration radius difference was lower than 0.01 Ångström. We also removed energetically high-lying local minima, if the relative total GFN-*x*TB energy with respect to the energetically lowest-lying structure was higher than  $5 \times N$  kcal/mol, where  $N$  is the number of molecules in the cluster.

The next step was optimization at the  $\omega$ B97X-D/6-31++g\*\* level of theory<sup>10</sup> with very tight optimization criteria. However, not all structures from the GFN-*x*TB step were used

due to a large amount of minima configurations remaining that fulfilled all above listed conditions. First, we did a uniform sampling/selection of 50 structures based on their GFN- $x$ TB energy and radius of gyration. Second, after optimization of these 50 structures on DFT level of theory, we re-selected another 50 structures from the GFN- $x$ TB step around the structures chosen in the primary selection. This set formed the lowest-lying structures on DFT level of theory. Thus, we selected overall 100 structures after the GFN- $x$ TB step.

Finally, for few energetically lowest-lying cluster structures ( $0-2N$  kcal/mol, where  $N$  is the number of molecules in the cluster), we performed vibrational frequency analysis to obtain thermal corrections for the free energies. On top of the 2-5 lowest DFT free energy structures, we calculated the single point electronic energy corrections using DLPNO-CCSD(T)/aug-cc-pVTZ level of theory. The DLPNO single point energy and the DFT thermal correction were used to calculate the Gibbs free energy of the cluster. The Gibbs free binding energies for the global minimum energy clusters are calculated as:

$$\Delta G = G_{\text{cluster}} - \sum_i G_{\text{monomers},i}. \quad (1)$$

As mentioned, the Gibbs free binding energy is a sum of the DLPNO binding energy ( $\Delta E$ ) and the DFT thermal contribution ( $\Delta G_{\text{Thermal}}$ ), calculated as

$$\Delta G = \Delta E + \Delta G_{\text{Thermal}}. \quad (2)$$

Table S1 presents  $\Delta E$ ,  $\Delta G_{\text{Thermal}}$  and  $\Delta G$ . The compounds are referred to as follows: A=sulfuric acid, N=ammonia, D=dimethylamine, G=guanidine, B=bisulfate and P=proton. The corresponding cluster structures in xyz format are found in the supplementary zip folder.

**Table S1:** Binding energies ( $\Delta E$ , DLPNO), thermal contributions to the Gibbs free energy ( $\Delta G_{\text{Thermal}}$ , DFT) and Gibbs free binding energies ( $\Delta G$ , DLPNO//DFT). All values are in kcal/mol,  $\Delta G_{\text{Thermal}}$  and  $\Delta G$  are calculated at 298.15 using RRHO approximation.

Cluster	$\Delta E$	$\Delta G_{\text{Thermal}}$	$\Delta G$
1A1N	-16.433	9.674	-6.759
1A2N	-31.280	19.711	-11.569
1A3N	-43.184	33.445	-9.739
1A4N	-55.680	45.252	-10.427
2A1N	-46.742	25.380	-21.362
2A2N	-66.389	37.463	-28.926
2A3N	-82.373	50.157	-32.216
2A4N	-95.896	61.380	-34.515
3A1N	-67.730	37.106	-30.625
3A2N	-94.650	50.837	-43.813
3A3N	-119.675	63.878	-55.798
3A4N	-139.217	79.208	-60.009
4A1N	-89.101	51.613	-37.488
4A2N	-121.308	67.715	-53.593
4A3N	-147.440	79.872	-67.568
4A4N	-173.116	89.714	-83.402
2N	-3.187	6.934	3.747
3N	-10.703	19.198	8.495
4N	-16.595	29.850	13.254
1B1N	-10.519	11.742	1.224
1B2N	-18.836	20.001	1.165
1A1B1N	-59.246	27.076	-32.170
1A1B2N	-69.183	38.538	-30.645
2A1B1N	-97.249	41.036	-56.213
2A1B2N	-114.240	51.916	-62.324
2A1B3N	-131.945	65.654	-66.325
3A1B1N	-126.408	52.311	-74.098
3A1B2N	-151.355	67.207	-84.148
3A1B3N	-173.355	81.412	-91.942
3A1B4N	-196.468	97.104	-99.232
4A1B1N	-155.362	67.777	-87.585
4A1B2N	-179.504	80.065	-99.439
4A1B3N	-209.649	94.894	-114.756
4A1B4N	-224.474	105.423	-119.051
1P2N	-26.281	7.202	-19.079
1P3N	-46.015	18.098	-27.917
1P4N	-60.051	21.935	-32.830
1P5N	-75.667	34.809	-40.858

1A1P1N	-21.279	5.914	-15.365
1A1P2N	-55.088	19.524	-35.564
1A1P3N	-74.080	30.104	-43.975
1A1P4N	-90.996	39.969	-51.027
1A1P5N	-108.197	51.044	-56.952
2A1P1N	-47.851	20.672	-27.180
2A1P2N	-82.511	33.532	-48.978
2A1P3N	-115.137	47.440	-67.697
2A1P4N	-132.884	56.720	-76.164
2A1P5N	-150.004	65.851	-84.153
3A1P3N	-138.154	59.693	-78.461
3A1P4N	-168.922	73.662	-95.260
3A1P5N	-187.215	85.253	-101.962
4A1P4N	-192.803	86.155	-106.648
4A1P5N	-228.170	101.998	-126.172
1A1D	-24.819	11.284	-13.535
1A2D	-40.462	23.234	-17.227
1A3D	-57.275	36.394	-20.881
1A4D	-71.532	50.226	-21.306
2A1D	-58.921	26.287	-32.634
2A2D	-90.137	41.564	-48.574
2A3D	-111.094	55.169	-55.925
2A4D	-126.846	66.712	-60.134
3A1D	-84.855	40.667	-44.188
3A2D	-120.432	55.775	-64.657
3A3D	-154.415	71.166	-83.249
3A4D	-178.359	85.309	-93.051
4A1D	-105.456	54.449	-51.007
4A2D	-144.846	69.843	-75.004
4A3D	-179.242	83.415	-95.827
4A4D	-213.369	97.940	-115.429
2D	-5.042	9.366	4.324
3D	-14.493	20.991	6.498
4D	-23.794	29.633	5.839
1B1D	-13.207	12.991	-0.216
1B2D	-24.328	23.172	-1.156
1A1B1D	-70.197	28.490	-41.707
1A1B2D	-84.320	41.011	-43.309
2A1B1D	-106.951	41.579	-65.371
2A1B2D	-133.061	56.689	-76.372
2A1B3D	-154.180	70.495	-83.686
3A1B1D	-134.801	54.872	-79.929
3A1B2D	-170.166	70.638	-99.528
3A1B3D	-195.297	83.973	-111.324
3A1B4D	-219.245	101.100	-118.145

4A1B1D	-162.690	68.157	-94.534
4A1B2D	-207.598	86.072	-121.527
4A1B3D	-241.279	101.698	-139.580
4A1B4D	-273.940	118.960	-154.980
1P2D	-24.908	9.182	-15.726
1P3D	-44.506	20.311	-24.195
1P4D	-56.313	31.010	-25.304
1P5D	-67.728	44.177	-23.551
1A1P1D	-19.343	8.990	-10.354
1A1P2D	-63.088	22.505	-40.583
1A1P3D	-92.305	37.373	-54.932
1A1P4D	-111.390	49.229	-61.934
1A1P5D	-129.838	61.392	-68.446
2A1P1D	-39.520	21.241	-18.279
2A1P2D	-91.584	35.393	-56.191
2A1P3D	-133.102	50.947	-82.155
2A1P4D	-162.995	65.504	-97.491
2A1P5D	-185.235	79.626	-105.609
3A1P3D	-157.622	65.200	-92.422
3A1P4D	-199.011	80.104	-118.907
3A1P5D	-230.617	97.488	-133.130
4A1P4D	-223.576	93.344	-130.233
4A1P5D	-263.655	107.864	-155.790
1A1G	-30.345	10.044	-20.302
1A2G	-52.747	23.937	-28.809
1A3G	-76.585	38.060	-38.525
1A4G	-97.699	51.765	-45.934
2A1G	-65.589	27.227	-38.362
2A2G	-106.176	37.930	-68.247
2A3G	-129.138	55.360	-73.778
2A4G	-150.019	66.192	-83.826
3A1G	-91.208	39.927	-51.281
3A2G	-138.199	55.189	-83.011
3A3G	-178.926	67.737	-111.189
3A4G	-214.788	81.387	-133.401
4A1G	-113.420	53.471	-59.948
4A2G	-161.413	67.611	-93.802
4A3G	-213.363	82.747	-130.616
4A4G	-269.588	99.840	-169.748
2G	-13.567	11.328	-2.239
3G	-27.759	24.688	-3.071
4G	-49.213	38.883	-10.330

1B1G	-21.563	10.558	-11.231
1B2G	-44.943	27.296	-17.217
1A1B1G	-71.817	21.375	-50.441
1A1B2G	-117.100	42.689	-58.651
2A1B1G	-150.481	56.253	-74.411
2A1B2G	-178.731	69.906	-104.285
2A1B3G	-99.152	40.500	-111.669
3A1B1G	-158.606	54.321	-94.229
3A1B2G	-197.222	73.133	-124.089
3A1B3G	-223.469	85.811	-150.197
3A1B4G	-184.365	72.696	-173.899
4A1B1G	-233.876	83.680	-108.825
4A1B2G	-266.749	97.873	-137.658
4A1B3G	-275.856	101.957	-168.876
4A1B4G	-314.018	113.462	-200.556
1P2G	-28.627	9.909	-18.336
1P3G	-52.232	21.005	-31.227
1P4G	-72.036	31.573	-40.463
1P5G	-88.317	47.432	-40.885
1A1P1G	-19.917	10.449	-9.206
1A1P2G	-69.606	20.300	-49.306
1A1P3G	-103.704	32.990	-70.714
1A1P4G	-120.782	49.165	-71.617
1A1P5G	-148.753	64.248	-84.505
2A1P1G	-41.233	20.834	-19.866
2A1P2G	-93.668	35.120	-58.548
2A1P3G	-144.459	50.910	-93.550
2A1P4G	-180.443	64.274	-116.170
2A1P5G	-206.754	80.566	-126.188
3A1P3G	-169.544	66.634	-102.909
3A1P4G	-221.984	83.139	-138.845
3A1P5G	-258.888	93.617	-165.271
4A1P4G	-251.241	95.151	-156.090
4A1P5G	-293.456	108.633	-184.823
2A	-18.958	11.410	-7.547
3A	-37.797	24.634	-13.163
4A	-56.320	34.358	-21.962
1A1B	-48.364	14.530	-33.834
2A1B	-78.291	27.099	-51.192
3A1B	-105.120	39.503	-65.617
4A1B	-124.215	52.852	-71.363

---

## Evaporation Rates

The evaporation rates of the clusters are obtained from the Gibbs free binding energies  $\Delta G$  of the evaporating cluster and its products as

$$\gamma_{(i+j) \rightarrow i,j} = \beta_{i,j} \frac{p_{\text{ref}}}{k_{\text{B}}T} \exp\left(\frac{\Delta G_{i+j} - \Delta G_i - \Delta G_j}{k_{\text{B}}T}\right). \quad (3)$$

The collision coefficients for neutral-neutral collisions are computed from kinetic gas theory as

$$\beta_{i,j} = \left(\frac{3}{4\pi}\right)^{1/6} \left[6k_{\text{B}}T \left(\frac{1}{m_i} + \frac{1}{m_j}\right)\right]^{1/2} \left(V_i^{1/3} + V_j^{1/3}\right)^2, \quad (4)$$

where  $m_i$  and  $V_i$  are the mass and volume of cluster  $i$ , respectively. The volumes are calculated using bulk liquid densities (1830, 696, 680 and 1550  $\frac{\text{kg}}{\text{m}^3}$  for sulfuric acid, ammonia, dimethylamine and guanidine, respectively) assuming spherical clusters and ideal mixing.

In collisions between ions and neutral molecules or clusters, the collision cross section is larger than that predicted from the physical dimensions of the colliding systems due to their long-range attraction.<sup>11</sup> For the neutral-ion collision coefficients we have applied the approach by Su and Chesnavich,<sup>12</sup> who performed trajectory simulations of collisions between a point charge and a rigidly rotating molecule. The collision frequency is dependent on three reduced parameters:

$$\begin{aligned} \beta_{i,j}^L &= q_i \left(\frac{1}{m_i} + \frac{1}{m_j}\right)^{1/2} \left(\frac{\pi\alpha_j}{\epsilon_0}\right)^{1/2} \\ I^* &= \frac{\mu_j I}{\alpha_j q_i} \left(\frac{1}{m_i} + \frac{1}{m_j}\right) \\ x &= \frac{\mu_j}{(8\pi\epsilon_0\alpha_j k_{\text{B}}T)^{1/2}} \end{aligned}$$

where  $q_i$  is the charge of the ion,  $\alpha_j$ ,  $\mu_j$ , and  $I$  are the polarizability, dipole moment, and moment of inertia of the neutral molecule, respectively, and  $\epsilon_0$  is the vacuum permittivity. At low values of  $I^*$ , *i.e.* when  $I^* < \frac{0.7+x^2}{2+0.6x}$ , the collision rate was observed to be independent

of  $I^*$ , and a fit to the simulated data produced the parametrization

$$\beta_{i,j} = \begin{cases} \beta_{i,j}^L (0.4767x + 0.6200), & x \geq 2 \\ \beta_{i,j}^L \left( \frac{(x+0.5090)^2}{10.526} + 0.9754 \right), & x < 2. \end{cases} \quad (5)$$

The parametrization has been compared with experimental collision rates and was found to give a good correspondence.<sup>11</sup>

Figure S1 shows the evaporation rates of all studied clusters.

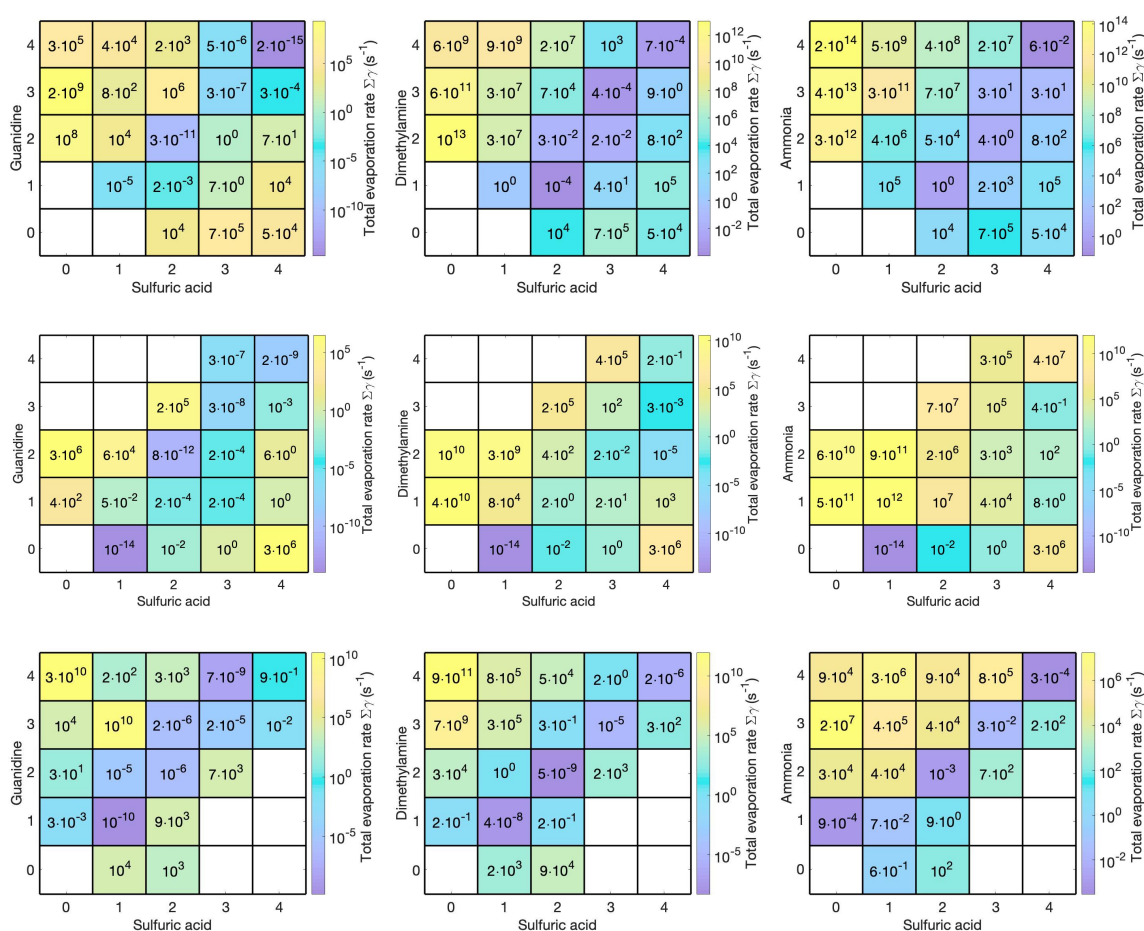


Figure S1: Evaporation rates of sulfuric acid clusters with guanidine (left), dimethylamine (middle) and ammonia (right). First row: neutral clusters, second row: anionic cluster (each cluster contains one bisulfate ion) and third row: cationic clusters (each cluster contains one protonated base).

## Cluster Population Dynamics Simulations

The time evolution and behavior of a population of clusters of different sizes and compositions is obtained by integrating the time derivatives of the cluster concentrations using the Atmospheric Cluster Dynamics Code.<sup>13</sup> These birth–death equations include all possible processes where the clusters can be formed or destroyed. For cluster  $i$  of a given composition, the time derivative is

$$\begin{aligned} \frac{dC_i}{dt} = & \frac{1}{2} \sum_{j < i} \beta_{j,(i-j)} C_j C_{(i-j)} + \sum_j \gamma_{(i+j) \rightarrow i,j} C_{(i+j)} - \sum_j \beta_{i,j} C_i C_j - \\ & \frac{1}{2} \sum_{j < i} \gamma_{i \rightarrow j,i-j} C_i + S_i - L_i C_i, \end{aligned} \quad (6)$$

where  $C_i$  is the concentration of cluster  $i$ ,  $\beta_{i,j}$  is the collision rate coefficient between  $i$  and  $j$ ,  $\gamma_{(i+j) \rightarrow i,j}$  is the evaporation rate coefficient of cluster  $(i+j)$ ,  $S_i$  is an external source term, and  $L_i$  is an external loss term corresponding to coagulation onto pre-existing surfaces. The loss rate  $L_i$  was assumed to depend on cluster size according to the parametrization by Lehtinen *et al.*<sup>14</sup> The reference loss rate, corresponding to a sulfuric acid molecule, was set to  $10^{-3} \text{ s}^{-1}$ , and the scavenging coefficient  $m$  to  $-1.6$  corresponding to typical atmospheric conditions. ACDC is available from the authors upon request.

## Boundary Conditions

By boundary conditions we refer to the smallest clusters outside of the simulation box which can be assumed to be stable (evaporation rate  $\ll 10^{-1} \text{ s}^{-1}$ ). This selection has been done based on the evaporation rates presented in Figure S1. The following boundary conditions are used in the particle formation simulations:

- Neutral sulfuric acid–guanidine: 5A4G and 4A5G
- Anionic sulfuric acid–guanidine: 5A1B4G and 4A1B5G
- Cationic sulfuric acid–guanidine: 5A5G1P and 4A6G1P

- Neutral sulfuric acid–dimethylamine: 5A4D
- Anionic sulfuric acid–dimethylamine: 5A1B4D
- Cationic sulfuric acid–dimethylamine: 4A6D1P
- Neutral sulfuric acid–ammonia: 5A4N
- Anionic sulfuric acid–dimethylamine: 5A1B3N
- Cationic sulfuric acid–dimethylamine: 5A5N1P.

## Electrically Neutral Particle Formation

Based on the Gibbs free energies, we simulated new-particle formation rates with the ACDC model and compared the results to atmospheric measurements,<sup>15–17</sup> investigating which simulated base concentrations yield NPF rates close to the measurements. It should be noted that our simulations consider only a single base at a time and the effect of hydration has not been considered, whereas atmospheric measurements include contributions of multiple compounds and synergistic effects might have a significant role. Figure S2 shows the simulated NPF rates considering only electrically neutral molecular clusters for each base, together with the rates deduced from measurements. The figure includes NPF rates at four different base concentrations that yield results close to the experimental rates at atmospherically relevant sulfuric acid vapor concentrations.

In the case of guanidine and sulfuric acid, a guanidine concentration of 0.001–1 ppt<sub>v</sub> is needed to yield NPF rates of the magnitude of the observations. In the sulfuric acid–dimethylamine case, dimethylamine concentration of 0.1–100 ppt<sub>v</sub> is needed, and ammonia-enhanced particle formation requires 10<sup>4</sup>–10<sup>7</sup> ppt<sub>v</sub> of ammonia. However, as stated above, these results address two-component systems: it has been demonstrated that the presence of ammonia increases particle formation when added to a two-component sulfuric acid–amine system.<sup>2,18,19</sup> Due to the fact that in the atmosphere ammonia is in practice always present, it can thus be assumed that even lower dimethylamine concentrations can produce NPF rates of the order of the observations.

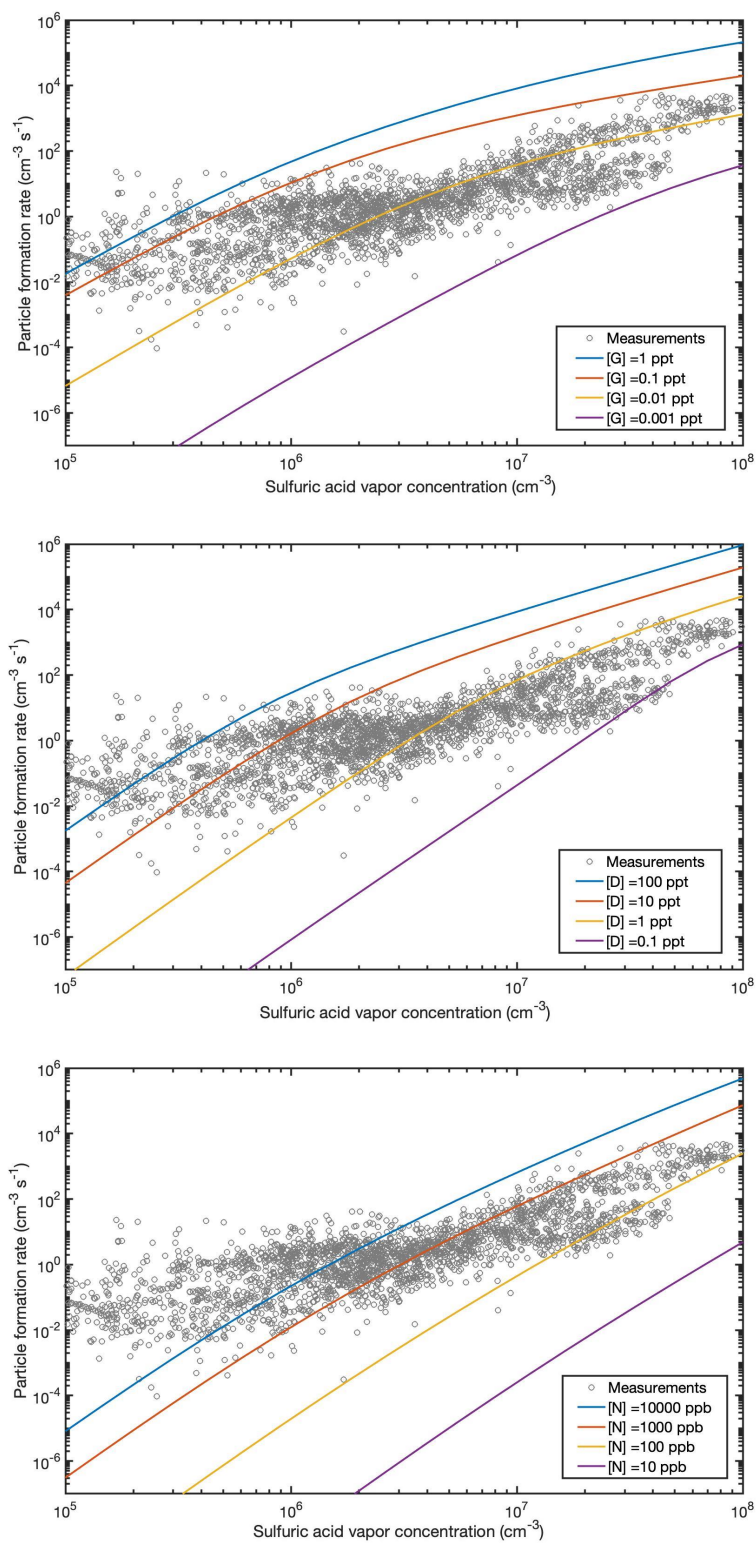


Figure S2: Simulated (lines) and observed (markers) new-particle formation rates as a function of sulfuric acid vapor concentration. Different base concentrations are used for guanidine (top), dimethylamine (middle) and ammonia (bottom).

## References

- (1) Myllys, N.; Ponkkonen, T.; Passananti, M.; Elm, J.; Vehkamäki, H.; Olenius, T. Guanine: A Highly Efficient Stabilizer in Atmospheric New-Particle Formation. *J. Phys. Chem. A* **2018**, *122*, 4717–4729.
- (2) Myllys, N.; Chee, S.; Olenius, T.; Lawler, M.; Smith, J. N. Molecular-Level Understanding of Synergistic Effects in Sulfuric Acid–Amine–Ammonia Mixed Clusters. *J. Phys. Chem. A* **2019**, *0*, just accepted.
- (3) Olenius, T.; Kupiainen-Määttä, O.; Ortega, I. K.; Kurtén, T.; Vehkamäki, H. Free Energy Barrier in the Growth of Sulfuric Acid–Ammonia and Sulfuric Acid–Dimethylamine Clusters. *J. Chem. Phys.* **2013**, *139*, 084312.
- (4) Karaboga, D.; Basturk, B. On the Performance of Artificial Bee Colony (ABC) Algorithm. *Appl. Soft Comput.* **2008**, *8*, 687–697.
- (5) Zhang, J.; Dolg, M. ABCluster: The Artificial Bee Colony Algorithm for Cluster Global Optimization. *Phys. Chem. Chem. Phys.* **2015**, *17*, 24173–24181.
- (6) Zhang, J.; Dolg, M. Global Optimization of Clusters of Rigid Molecules using the Artificial Bee Colony Algorithm. *Phys. Chem. Chem. Phys.* **2016**, *18*, 3003–3010.
- (7) Vanommeslaeghe, K.; Hatcher, E.; Acharya, C.; Kundu, S.; Zhong, S.; Shim, J.; Darian, E.; Guvench, O.; Lopes, P.; Vorobyov, I.; Jr., A. D. M. CHARMM General Force Field: A Force Field for Drug-Like Molecules Compatible with the CHARMM All-Atom Additive Biological Force Fields. *J. Comput. Chem.* **2010**, *31*, 671–690.
- (8) Yu, W.; He, X.; Vanommeslaeghe, K.; Jr., A. D. M. Extension of the CHARMM General Force Field to Sulfonyl-Containing Compounds and Its Utility in Biomolecular Simulations. *J. Comput. Chem.* **2012**, *33*, 2451–2468.

- (9) Grimme, S.; Bannwarth, C.; Shuskov, P. A Robust and Accurate Tight-Binding Quantum Chemical Method for Structures, Vibrational Frequencies, and Noncovalent Interactions of Large Molecular Systems Parametrized for all spd-Block Elements ( $Z = 1-86$ ). *J. Chem. Theory Comput.* **2017**, *13*, 1989–2009.
- (10) Chai, J.-D.; Head-Gordon, M. Long-Range Corrected Hybrid Density Functionals with Damped Atom-Atom Dispersion Corrections. *Phys. Chem. Chem. Phys.* **2008**, *10*, 6615–6620.
- (11) Kupiainen-Määttä, O.; Olenius, T.; Kurtén, T.; Vehkamäki, H. CIMS Sulfuric Acid Detection Efficiency Enhanced by Amines Due to Higher Dipole Moments: A Computational Study. *J. Phys. Chem. A* **2013**, *117*, 14109–14119.
- (12) Su, T.; Chesnavich, W. J. Parametrization of the Ion–Polar Molecule Collision Rate Constant by Trajectory Calculations. *J. Chem. Phys.* **1982**, *76*, 5183–5185.
- (13) McGrath, M. J.; Olenius, T.; Ortega, I. K.; Loukonen, V.; Paasonen, P.; Kurtén, T.; Kulmala, M.; Vehkamäki, H. Atmospheric Cluster Dynamics Code: a Flexible Method for Solution of the Birth–Death Equations. *Atmos. Chem. Phys.* **2012**, *12*, 2345–2355.
- (14) Lehtinen, K. E.; Maso, M. D.; Kulmala, M.; Kerminen, V.-M. Estimating Nucleation Rates from Apparent Particle Formation Rates and vice versa: Revised Formulation of the Kerminen–Kulmala Equation. *J. Aerosol Sci.* **2007**, *38*, 988–994.
- (15) Paasonen, P. et al. On the Roles of Sulphuric Acid and Low-Volatility Organic Vapours in the Initial Steps of Atmospheric New Particle Formation. *Atmos. Chem. Phys.* **2010**, *10*, 11223–11242.
- (16) Sihto, S.-L.; Kulmala, M.; Kerminen, V.-M.; Dal Maso, M.; Petäjä, T.; Riipinen, I.; Korhonen, H.; Arnold, F.; Janson, R.; Boy, M.; Laaksonen, A.; Lehtinen, K. E. J. Atmospheric Sulphuric Acid and Aerosol Formation: Implications from Atmospheric

- Measurements for Nucleation and Early Growth Mechanisms. *Atmos. Chem. Phys.* **2006**, *6*, 4079–4091.
- (17) Kuang, C.; McMurry, P. H.; McCormick, A. V.; Eisele, F. L. Dependence of Nucleation Rates on Sulfuric Acid Vapor Concentration in Diverse Atmospheric Locations. *J. Geophys. Res. Atmos.* **2008**, *113*.
- (18) Yu, H.; McGraw, R.; Lee, S.-H. Effects of Amines on Formation of Sub-3 nm Particles and Their Subsequent Growth. *Geophys. Res. Lett.* **2012**, *39*, 2.
- (19) Glasoe, W.; Volz, K.; Panta, B.; Freshour, N.; Bachman, R.; Hanson, D.; McMurry, P.; Jen, C. Sulfuric Acid Nucleation: An Experimental Study of the Effect of Seven Bases. *J. Geophys. Res. Atmos.* **2015**, *120*, 1933–1950.